Submitted to The Astrophysical Journal

History of Galaxy Interactions and Their Impact on Star Formation over the Last 7 Gyr from GEMS

Shardha Jogee [1], Sarah H. Miller [1], Kyle Penner [1], Rosalind E. Skelton [3], Chris Conselice [2], Rachel S. Somerville [3], Eric F.Bell [3], Xian Zhong Zheng [16], Hans-Walter Rix [3], Aday R. Robaina [3], Fabio D. Barazza [6], Marco Barden [15], Andrea Borch [3], Steven V.W. Beckwith [5], John A. R.Caldwell [7], Boris Häußler [2], Catherine Heymans [13,14], Knud Jahnke [3], Daniel H. McIntosh [8], Klaus Meisenheimer [3], Casey Papovich [4], Chien Y. Peng [9], Sebastian F. Sanchez [10], Lutz Wisotzki [11], Christian Wolf [12]

sj@astro.as.utexas.edu

ABSTRACT

We explore the frequency and impact of strong interactions on the star formation rate (SFR) of galaxies over $z \sim 0.24$–0.80 (lookback time $\sim$ 3–7 Gyr), based on *HST* ACS, Combo-17, and Spitzer 24 μm data of ~ 3800 ($M \geq 1 \times 10^9$ $M_\odot$) galaxies in the GEMS survey. Two independent methods are used to identify strongly interacting galaxies: a tailored visual classification system complemented with spectrophotometric redshifts and stellar masses, as well as the CAS merger criterion ($A > 0.35$ and $A > S$). The strongly interacting galaxies are candidates for a recent/ongoing interaction of mass ratio $M1/M2 > 1/10$. Our

[1]Department of Astronomy, University of Texas at Austin, 1 University Station C1400, Austin, TX 78712-0259

[2]School of Physics and Astronomy, The University of Nottingham, University Park, Nottingham NG7 2RD, UK

[3]Max-Planck-Institut für Astronomie, Königstuhl 17, D-69117, Heidelberg, Germany

[4]Department of Astronomy, University of Arizona, Steward Observatory, 933 N. Cherry Avenue, Tucson, AZ 85721

[5]Department of Physics and Astronomy, Johns Hopkins University, Charles and 4th Street, Baltimore, MD 21218

[6]Laboratoire d'Astrophysique, École Polytechnique Fédérale de Lausanne (EPFL), Observatoire, 1290 Sauverny, Switzerland

[7]University of Texas, McDonald Observatory, Fort Davis TX, 79734 USA

[8]Department of Astronomy, University of Massachusetts, 710 North Pleasant Street, Amherst, MA 01003, USA

[9]NRC Herzberg Institute of Astrophysics, Victoria, Canada

[10]Centro Astronmico Hispano Alemn, Calar Alto, CSIC-MPG, C/Jess Durbn Remn 2-2, E-04004 Almeria, Spain

[11]Astrophysikalisches Institut Potsdam, An der Sternwarte 16, D-14482 Potsdam, Germany

[12]Astrophysics, University of Oxford, Keble Road, Oxford OX1 3RH, U.K.

[13]Department of Physics and Astronomy, University of British Columbia, 6224 Agricultural Road, Vancouver, V6T 1Z1, Canada

[14]Institut d'Astrophysique de Paris, UMR7095 CNRS, 98 bis bd Arago, 75014 Paris, France

[15]Institute for Astro- and Particle Physics, University of Innsbruck, Technikerstr. 25/8, A-6020 Innsbruck, Austria

[16]Purple Mountain Observatory, Nanjing, China.

results are: (1) The CAS criterion ($A > 0.35$ and $A > S$) picks only 40% to 50% of the galaxies visually-classified as strongly interacting galaxies, but is contaminated by a large number of non-interacting dusty, star-forming galaxies. This contamination must be borne in mind by studies that use CAS in blind automated mode. (2) The observed fraction f of strongly interacting systems among $\sim$ 800 high mass ($M \geq 2.5 \times 10^{10}$ $M_{\odot}$) galaxies varies from 6% $\pm$ 2% to 12% $\pm$ 4% over $z \sim 0.24$–0.80 (lookback time $\sim$ 3–7 Gyr), as averaged over every Gyr bin. For an assumed visibility timescale of $\sim$ 0.3 Gyr, the results yield an interaction rate $R \sim$ a few $\times 10^{-4}$ galaxies Gyr^{-1} Mpc^{-3}, and imply that each massive galaxy has undergone at least 1.3 interactions of mass ratio $> 1/10$ since $z \sim 0.80$. Thus interactions of mass ratio $> 1/10$ are prevalent over the last 7 Gyr, albeit at lower frequency than at $z > 2$, where a larger fraction ($f > 40\%$) is reported. (3) For a subset of the strongly interacting high mass galaxies, stellar masses and unique morphological tell-tale signatures enable us to decide whether the system is a major ($M1/M2 \geq 1/4$) or minor ($1/10 \leq M1/M2 < 1/4$) interaction. The resulting fraction of major and minor interactions is $\geq$ 2.5% and 4.0%, respectively. For an assumed visibility timescale of $\sim$ 0.3 Gyr, this implies that each massive galaxy has undergone at least 0.33 major and 0.60 minor interactions since $z \sim 0.80$ (lookback time $\sim$ 7 Gyr). (4) We compare our results on the interaction history of high mass galaxies to predictions from different ΛCDM-based simulations of galaxy evolution. Fair agreement is found with a subset of simulations, but some SPH-based simulations seriously underpredict the interaction rate R. (5) Among $\sim$ 3800 galaxies with $M \geq 1.0 \times 10^{9}$ $M_{\odot}$, the UV-based and UV+IR-based average SFRs are only modestly enhanced in strongly interacting galaxies, compared to non-interacting ' 'normal' galaxies. Our results of a modest interaction fraction f and a modest enhancement in SFR from interactions culminate in our finding that strongly interacting systems only account for a small fraction ($< 30\%$) of of the cosmic SFR density over $z \sim 0.24$–0.80 (lookback time $\sim$ 3–7 Gyr). In effect, contrary to common lore, the behavior of the cosmic SFR density over the last 7 Gyr is predominantly shaped by normal galaxies rather than strongly interacting galaxies.

Subject headings: galaxies: fundamental parameters — galaxies: structure — galaxies: kinematics and dynamics — galaxies: evolution

1. Introduction

Hierarchical ΛCDM (LCDM) models provide a successful paradigm for the growth of dark matter on large scales. The evolution of galaxies within ΛCDM cosmogonies depends on the baryonic merger history, the star formation (SF) history, the nature and level of feedback from supernovae and AGN, the redistribution of angular momentum via bars or mergers, and other aspects of the baryonic physics. Empirical constraints on the fate of the baryonic component are key, therefore, for developing a coherent picture of galaxy evolution. They also provide important tests for semi-analytical models (e.g., Kauffmann et al. 1993; Somerville & Primack 1999; Cole et al. 2000; Benson et al. 2005; Hopkins et al. 2007) and cosmological hydrodynamical simulations (e.g., Navarro & Steinmetz 2000; Murali et al. 2002; Governato et al. 2004; Robertson et al. 2004; Maller et al. 2006; Springel et al. 2007) of galaxy evolution within ΛCDM cosmogonies. In fact, empirical constraints on the interaction and SF history of baryons can help to resolve several major areas of discord between observations and hierarchical ΛCDM models of galaxy evolution, such as the angular momentum crisis, the problem of bulgeless galaxies (Navarro & Benz 1991; Burkert & D'Onghia 2004; Kautsch et al. 2006; Barazza, Jogee, & Marinova 2007), and the substructure or missing satellite problem.

The interaction history of galaxies impacts the mass assembly, star formation history, AGN activity, and structural evolution of galaxies. At redshifts $z > 2$, corresponding to lookback times $T_{\rm back} > 10.4$ Gyr[17], observations suggest a large merger frequency of $> 40\%$ among massive galaxies (e.g. Conselice et al. 2003; Patton et al. 2000; Le Fevre et al. 2000). At $z < 1$, the volume sampled and sample size used by earlier studies were small leading to uncertain and conflicting results (Conselice et al. 2003; Lin 2004 ; Patton et al 2002; Casato 2005; dePropis 07). Recent studies based on larger samples have employed different methods to characterize the interaction history of galaxies at $z < 1$. Studies based on Gini-M20 coefficients report a fairly constant fraction ($\sim 7 \pm 0.2$ %) of disturbed galaxies over z$\sim$ 0.2 to 1.2 among bright galaxies (Lotz et al 2008) in the AEGIS survey. Other studies based on close pairs report a major merger frequency of $\sim 2\%$ to 10% over z$\sim$ 0.2 to 1.2 (Kartaltepe et al 2008) and $\sim 5\%$ for massive galaxies at z$\sim$ 0.4 to 0.8 (Bell et al 2006).

Studies to date have brought important insights but face several limitations. The use of automated parameters, such as CAS asymmetry A and clumpiness parameters or Gini-M20 coefficients, to identify interacting galaxies can fail to pick stages of major or minor interaction where distortions do not dominate the total light contribution (§ 3.3). Comparison with simulations suggest that the CAS criterion ($A > 0.35$ and $A > S$) capture major mergers

[17]We assume in this paper a flat cosmology with $\Omega_M = 1 - \Omega_\Lambda = 0.3$ and H_0 =70 km s^{-1} Mpc^{-1}.

about 1/3 of the time, while the eye is sensitive to major merger features over twice as long (e.g., Conselice 2006; § 3.3). To complicate matters, automated asymmetry parameters can also capture non-interacting galaxies hosting small-scale asymmetries that are produced by stochastic star formation (§ 3.3). In the case of studies based on close (separation $\sim$ 5 to 30 kpc) pairs, the translation of the pair frequency into a merger rate is non-trivial due to several factors. The uncertainties in the photometric redshifts can lead to false pairs caused by chance line-of-sight projection. Secondly, even pairs with members at the same redshift may not be gravitationally bound, and may therefore not evolve into a strong interaction or merger in the future. Thirdly, gravitationally bound pairs captured by this method sample different phases of an interaction depending on the separation and any merger rate inferred depends on the separation, orbital eccentricity, and orbital geometry.

In this paper, we present a complementary study of the frequency and impact of strong galaxy interactions on the SF activity of galaxies over $z \sim 0.24$–0.80 (lookback times of 3–7 Gyr) using *HST* ACS, Combo-17, and Spitzer 24 μm data of $\sim$ 3800 galaxies in the GEMS survey. This study complements existing studies in several ways.

1. We use a large sample of $\sim$ 3800 ($M \geq 1 \times 10^9\ M_\odot$) galaxies and $\sim$ 800 high mass ($M \geq 2.5 \times 10^{10}\ M_\odot$) galaxies for robust number statistics (§ 2). Two independent methods are used to identify strongly interacting galaxies: a tailored visual classification system complemented with spectrophotometric redshifts and stellar masses (§ 3.2), as well as automated CAS asymmetry and clumpiness parameters (§ 3.3). This allows the first systematic comparison to date between CAS-based and visual classification results (§ 4.2). We also try to assess the impact of moderate bandpass shifts and surface brightness dimming (§ 4.1).
2. We set up the visual classification system (§ 3.2) so as to target strong interactions with mass ratio $M1/M2 > 1/10$. While many earlier studies focused on major mergers, it is important to constrain minor mergers as well, since minor mergers dominate the merger rates in LCDM models at $z < 1$.
3. We compare the observed fraction f and inferred merger rate R to a suite of ΛCDM-based simulations of galaxy evolution, including both semi-analytical and hydrodynamic SPH-based simulations (§ 4.4). To our knowledge, such extensive comparisons have not been attempted to date, and are long overdue.
4. In § 4.6 to § 4.7, we investigate the impact of strong galaxy interactions on the SFR and cosmic SFR density of intermediate-to-high mass ($M \geq 1 \times 10^9\ M_\odot$) galaxies. In particular, we estimate the relative contributions of normal versus interacting galaxies to the cosmic SFR density. This question is of great astrophysical interest, particularly given that the cosmic SFR density is claimed to decline by a factor of 3 to 10 since $z \sim 1$ (e.g., Madau et al. 1996, 1998; Cowie et al. 1996; Flores et al. 1999; Haarrsma et

al. 2000). The idea that galaxy interactions enhance the SFR of galaxies and trigger strong nuclear starbursts is well established from observations (e.g. Larson & Tinsley 1978; Joseph & Wright 1985; Kennicutt et al. 1987; Barton et al 2003) and simulations (e.g., Negroponte & White 1983; Hernquist 1989; Barnes & Hernquist 1991, 1996; Mihos & Hernquist 1994, 1996; Barnes 2004; Springel, Di Matteo & Hernquist 2005). However, simulations cannot robustly predict the impact of galaxy interactions on the SF activity of galaxies over the last 7 Gyr, since both the SFR and properties of the remnants in simulations are highly sensitive to the stellar feedback model, the bulge-to-disk (B/D) ratio, the gas mass fractions, and orbital geometry (e.g., Cox et al 2006; di Matteo et al. 2007).

2. Dataset and Sample Selection

This study uses data from the Galaxy Evolution from Morphology and SEDS (GEMS; Rix et al. 2004) survey, which provides high resolution *Hubble Space Telescope (HST)* Advanced Camera for Surveys (ACS) images in the F606W and F850LP filters over an 800 arcmin^2 ($\sim 28' \times 28'$) field centered on the Chandra Deep Field-South (CDF-S). Accurate spectrophotometric redshifts [$\delta_z/(1+z) \sim 0.02$ down to $R_{\rm Vega} = 24$] and spectral energy distributions, based on 5 broad bands ($UBVRI$) and 12 medium band filters, are available from the COMBO-17 project (Wolf et al. 2004). The ACS data reach a limiting 5 σ depth for point sources of 28.3 and 27.1 AB mag in F606W and F850LP, respectively (Rix et al. 2004). The effective point spread function (PSF) in a single F606W image is $\sim 0\farcs07$, corresponding to 260 pc at $z \sim 0.24$ and 520 pc at $z \sim 0.80$. In addition to HST ACS imaging, the GEMS field has panchromatic coverage which includes *Spitzer* (Rieke et al. 2004; Papovich et al. 2004) and *Chandra* data

We use stellar masses from Borch et al. (2006). We refer the reader to the latter publication for a detailed description and provide only a brief summary here. Objects were classified as main sequence, stars, white dwarfs, galaxies, and quasars using color indices and their photometric redshifts were estimated using simple dust-reddened single-burst SED templates (Wolf et al. 2004). For galaxies and quasars, the joint probability of a given redshift and a given rest-frame SED is derived and this procedure provides a minimum error variance estimation of both the redshift and the SED template. Once the redshfit has been estimated, the SEDs in 17 bands were fitted with a new set of template SEDs with more plausible SF histories in order to derive a stellar M/L (Borch et al. 2006). The library of SEDs is built using the PEGASE-code and the underlying SF histories are parameterized by the three-component model, with a Kroupa (Kroupa et al. 1993) initial mass function (IMF)

adopted in the mass regime 0.1–120 $M_{\odot}$.

We initially performed visual classification on and derived CAS parameters (§ 3) for both F606W and F850LP images. However, in this study we only present the results based on F606W images for the following reasons. The F606W images are ~ 1.2 magnitude deeper than the GEMS F850LP images and allow more reliable characterization of morphological features in the presence of cosmological surface brightness dimming at the rate of $(1+z)^{-4}$ (e.g., Barden et al. 2007). Furthermore, the low signal to noise in the F850LP images leads to large error bars on the asymmetry A and clumpiness S parameters generated by the CAS code, effectively making it impractical to use these values in CAS merger diagnostics (§ 3.3). When using the F606W images, we only include results over the redshift range $z \sim 0.24$–0.80 in order to ensure that the rest-frame wavelength $\lambda_{\rm rest}$ stays primarily in the optical band and does not shift to the far-UV. In the fourth redshift bin ($z \sim 0.6$ to 0.8) $\lambda_{\rm rest}$ shifts to the violet/near-UV (3700 Å to 3290 Å), but as we show in § 4.1, this does not impact the results significantly. We discard the last redshift bin ($z \sim 0.80$–0.95) where $\lambda_{\rm rest}$ shifts into the far-UV. In summary, based on the above considerations, we are left with a sample of ~ 4740 galaxies with $R_{\rm Vega} \leq 24$, over $z \sim 0.24$–0.80 ($T_{\rm back} \sim 3$–7 Gyr).

Figure 1 shows the rest-frame $U-V$ color plotted versus the stellar mass for this sample of ~ 4740 galaxies. The redshift interval is divided into four 1 Gyr bins. The diagonal line marks the separation of the red sequence and the blue cloud galaxies (BCG) at the average redshift $z_{\rm ave}$ of the bin. We use the definition in Borch et al. (2006) and Bell et al. (2004) for CDF-S:

$$(U-V)_{\rm rest} > 0.227\ \log({\rm M/M_{\odot}}) - 1.26 - 0.352{\rm z} \qquad (1)$$

The vertical lines on Figure 1 marks the mass completeness limit (Borch et al. 2006) for the red sequence galaxies. The blue cloud galaxies are complete well below this mass.

In this paper, we present further results for two samples of astrophysical interest. The first sample (henceforth sample S1) focuses on galaxies with high stellar mass ($M \geq 2.5 \times 10^{10}$ $M_{\odot}$; 804 galaxies). For this stellar mass range, the red sequence and blue cloud galaxies are both complete out to the highest redshift bin $z \sim 0.62$–0.80 for our sample, and theoretical predictions exist for comparison (see § 4.5) from semi-analytical models (e.g, Somerville et al. 2007; Hopkins et al. 2007; Benson et al. 2004) and hydrodynamical SPH simulations (e.g., Maller et al. 2006). Note that the survey has few galaxies above 10^{11} $M_{\odot}$ (Fig. 1), and hence the high mass sample ($M \geq 2.5 \times 10^{10}$ $M_{\odot}$) primarily involves galaxies in the range 2.5×10^{10} to 10^{11} $M_{\odot}$.

We also present selected results for the sample S2 of ~ 3860 galaxies with intermediate-

to-high stellar mass ($M \geq 1 \times 10^9\ M_\odot$). At this mass cutoff, the blue cloud is complete in our sample out to $z \sim 0.80$, while the red sequence is incomplete in the higher redshift bins. Results based on sample S2 are only presented for blue cloud galaxies and for properties that are not overly impacted by the missing red sequence galaxies.

3. Methodology: Identifying Disturbed and Normal Galaxies

3.1. Overview of the methodology

Galaxy mergers and interactions with mass ratio $M1/M2 > 1/10$ can have a significant impact on galaxy evolution. According to simulations, major mergers (defined as those with mass ratio $1/4 < M1/M2 \leq 1/1$) typically destroy disks, transforming them via violent relaxation, into systems with an $r^{1/4}$ de Vaucouleurs-type stellar profile, such as ellipticals (e.g., Negroponte & White 1983; Barnes & Hernquist 1991; Mihos & Hernquist 96; Struck 1997; Naab & Burkert 2001; but see Robertson et al 2004). These simulations suggest that ongoing/recent major mergers at $z \leq 1$ are associated with arcs, shells, ripples, tidal tails, large tidal debris, extremely asymmetric light distributions, double nuclei inside a common body, galaxies linked via tidal bridges of light, and galaxies enclosed within the same distorted envelope of light.

Minor mergers (defined as those with $1/10 < M1/M2 \leq 1/4$) of two spirals will not destroy the disk of the larger spiral (e.g., Hernquist & Mihos 1995; Smith et al. 1997; Jogee et al. 1999). Typically, the smaller companion sinks via dynamical friction, may excite warps, bars, spirals, and other non-axisymmetric perturbations, and leads to vertical heating, arcs, shells, ripples, tidal tails, tidal debris, warps, offset rings, highly asymmetric light distributions, etc (e.g., Quinn et al. 1993; Hernquist & Mihos 1995; Mihos et al. 1995; Quinn, Hernquist, & Fullagar 1993; Smith et al. 1997; Jogee et al. 1999; review by Jogee 2006 and references therein).

One goal of this paper is to identify strongly interacting systems, which are likely candidates for an ongoing or recent interaction of mass ratio $M1/M2 > 1/10$. As a guide to identifying these systems, we use the afore-mentioned morphological signatures seen in simulations. We employ two methods: a tailored visual classification system (§ 3.2 to § 4.1), and quantitative asymmetry (A), and clumpiness (S) parameters (§ 3.3) derived using the CAS code (Conselice et al. 2000). While many studies use only automated methods or visual classification, we choose to use both methods in order to better assess the systematics, and to test the robustness of our results.

To further constrain galaxy evolution, it would be useful if we could separate these

strongly interacting systems into major ($1/4 < M1/M2 \leq 1/1$) versus minor ($1/10 < M1/M2 \leq 1/4$) interactions. However, for many strongly interacting galaxies it is not possible to unambiguously make this distinction, since the morphological disturbances induced depend not only on the mass ratio of the progenitors, but also on the orbital geometry (prograde or retrograde), the gas mass fraction, and structural parameters (e.g., Mihos & Hernquist 96; Struck 1997; Naab & Burkert 2001; Mihos et al. 1995, di Matteo et al. 2007). In effect, many signatures could be caused by both major and minor interactions. Thus, we can only set lower limits to the fraction of major and minor interactions (see § 4.3), using a subset of the strongly interacting systems, which exhibit signatures unique to a major or minor interaction.

3.2. Visual Classification

We visually classified F606W images of the sample of ~ 4740 galaxies (§ 2) with $R_{\rm Vega} \leq 24$ in the redshift range $z \sim 0.24$–0.80. A small subset (below 4%) of galaxies could not be classified due to image defects, low signal to noise, highly compact appearance, etc.

As described in § 3.1, the main goal of this paper is to identify strongly interacting candidates, which are likely candidates for an ongoing or recent interaction of mass ratio $M1/M2 > 1/10$. We use the morphological signatures suggested by the simulations outlined in § 3.1 to identify these systems and assign them the visual class of strongly interacting ('Int') galaxies. Figure 2 shows examples in the four 1 Gyr redshift bins. In practice, during the visual classification, galaxies in the class 'Int' are sub-divided into two sub-groups, 'Int-1' and 'Int-2', described below.

1. 'Int-1': A galaxy is assigned an 'Int-1' class if it exhibits a strong morphological distortion, such as a warped disk, an offset ring, arcs, shells and ripples, tidal tails, large tidal debris, extremely asymmetric light distributions, double nuclei inside a common body, and tidally distorted bridges of light. The basic idea here is that 'Int-1' galaxies are unambiguous cases of strongly interacting galaxies, since they exhibit the morphological distortions induced by a strong gravitational disturbance. The class 'Int-1' is independent of the accuracy of the spectrophotometric redshift.
2. 'Int-2': A galaxy is assigned an 'Int-2' class if it shows no strong morphological distortions, but has a companion which satisfies three criteria: it is overlapping or in contact with it so that the two galaxies share a common envelope of light; it has the same Combo-17 spectrophotometric redshift within the accuracy $\delta_z/(1+z) \sim 0.02$ (§ 2); and its stellar mass ratio satisfies $M1/M2 > 1/10$. While the classification of a galaxy as Int-2 depends on spectrophotometric redshift, it is to be noted that 'Int-2' systems

are very unlikely to be be line-of-sight chance projection as the projected separation d of the two galaxies is typically < 5 kpc. This is a much smaller separation than that used in the identification of close pairs, where d is 5–20 kpc (Kartaltepe et al. 2008) or $d < 30$ kpc (Bell et al 2006).

Galaxies that show no evidence of an ongoing or recent interaction of mass ratio $> 1/10$, according to the above-established criteria, are classified as 'Normal' non-interacting galaxies. These galaxies may harbor very subtle distortions, but none of the type described in 'Int-1 and 'Int-2'. Figure 3 shows examples of 'Normal' galaxies in the four redshift bins. Galaxies in the class of 'normal non-interacting' are sub-divided into two sub-groups, 'E-to-Sd' and 'Irr', described below.

1. 'Irr': It is important to note that even non-interacting galaxies have some inherent level of small-scale asymmetries in optical light due to SF activity. In the case of low mass galaxies, further asymmetries may also arise due to the low ratio of rotational to random velocities, as is commonly seen in Im and Sm. These internally-triggered asymmetries due to SF in non-interacting galaxies differ in scale (few 100 pc vs several kpc) and morphology from the externally-triggered distortions typical of the 'Int-1' class. We classify non-interacting galaxies with such internally-triggered asymmetries as 'Irr' (see Figure 3). Such systems may get accidentally picked as 'interacting' in automated asymmetry-based codes (see § 4.2).
2. 'E-to-Sd': Galaxies are assigned the 'E to Sd' class if they are fairly symmetric, have Hubble types in the range E-to-Sd, and are not associated with any overlapping or contact companion.

In this paper, we are primarily concerned about the differences between three groups: the strongly interacting galaxies in class 'Int', the 'non-interacting E-to-Sd' galaxies, and the 'non-interacting Irr' galaxies. The details of how 'E-to-Sd' galaxies are further sub-divided into individual Hubble types do not have any major impact on our main results, and we only describe this sub-classification for the sake of completeness. In the Hubble classification system (1936), as we go from E to Sd, the bulge to disk (B/D) luminosity ratio, as well as smoothness and tightness of any spiral arms, are expected to decrease. The Hubble system works fairly well on average in field galaxies, although it may fail in clusters (e.g., Koopmann & Kenney 1998). We use conventional definitions (Binney & Merrifield 1998) for individual Hubble types (E, S0, Sa, Sb-Sc, and Sd). We assign an elliptical (E) type if a galaxy exhibits a smooth featureless appearance, show no disk signatures, such as a bar or spiral arms, and appear to be pure spheroids. We assign an S0 class if a galaxy hosts a smooth central brightness condensation, surrounded by an outer component, which is relatively featureless

(without spiral arms) and has a less steeply declining brightness profile (Binney & Merrifield 1998). We assign Sa, Sb-Sc, and Sd types using primarily visual estimates of the B/D ratio, and secondarily the smoothness/clumpiness of the disk. We do not accord much weight to the smoothness of spiral arms since the ACS F606W PSF ($\sim$ 260–560 pc at $z \sim 0.24$–0.80) precludes the identification of fine structures in the arms. In fact, at intermediate redshifts, where the faint smooth arms of Sa galaxies are not easily discernible, the distinction between E, S0, and Sa becomes blurred (see also § 4.1). However, this ambiguity between Es, S0s and Sas is not a problem for the subsequent analyses in this paper, since galaxies are grouped together either as 'E+S0+Sa' or 'E-to-Sd'. Results and further tests on the interaction history from visual classes are presented in § 4.1.

3.3. CAS

We derived the concentration C, asymmetry A, and clumpiness S (CAS) parameters by running the the CAS code (Conselice et al. 2000) on the F606W images. As is standard practice, the segmentation maps produced during the original source extraction (Caldwell et al. 2006) are used to mask neighbors on each ACS tile. The CAS code derives the asymmetry index A (Conselice 2003a) by rotating a galaxy image by 180 deg, subtracting the rotated image from the original image, summing the absolute intensities of the residuals, and normalizing the sum to the original galaxy flux. CAS improves the initial input center with the IRAF task 'imcenter' and then performs a further refinement within a 3×3 grid, picking the center that minimizes A. The CAS concentration index C (Bershady et al. 2000) is proportional to the logarithm of the ratio of the 80% to 20% curve of growth radii within 1.5 times the Petrosian inverted radius at $r(\eta = 0.2)$, normalized by a logarithm

$$C = 5 \times \log(\mathrm{r_{80\%}}/\mathrm{r_{20\%}}) \tag{2}$$

The clumpiness index S (Conselice 2003) is defined as the ratio of the amount of light contained in high-frequency structures to the total amount of light in the galaxy. In order to compute S, the CAS code first smooths the galaxy image, to produce a lower resolution image whose high-frequency structure has been washed out. The latter image is then subtracted from the original image to produce a residual map that contains only the high-frequency components of the galaxy's stellar light. The flux of this residual light is then summed and divided by the sum of the original galaxy image flux to obtain a galaxy's clumpiness (S) value. Tests on the interaction history from CAS are presented in § 4.2.

It has been argued that the criterion $A > 0.35$ and $A > S$ (henceforth referred to

as the CAS merger/interaction criterion) captures galaxies that exhibit large asymmetries produced by strong interactions (Conselice 2003a) . We will assess this in § 4.2.

4. Results and Discussion

4.1. Tests on the interaction fraction from visual classes

Fig 4 compares the fraction ($f_{\rm VC}$) of strongly interacting galaxies in the high mass sample, based on visual classification by 3 classifiers (SJ, SM, KP). The error bar plotted in each bin of size N is based on the binomial standard deviation $\sigma = [N\ f_{\rm VC}(1\text{-}f_{\rm VC})]^{1/2}$. The same trend is seen for all 3 classifiers and the maximum spread $\delta f_{\rm VC}/f_{\rm VC}$ in the 4 bins is 15%, 17%, 26% and 26%, respectively. In subsequent analyses, we conservatively adopt a dispersion of 30% on the mean $f_{\rm VC}$, as a measure of the inherent subjectivity in the visual classification.

Another key test is to assess the impact of redshift-dependent systematic effects, such as bandpass shifting. When using the F606W filter whose pivot wavelength is ~ 5915 Å, the rest frame wavelength ($\lambda_{\rm rest}$) corresponds to the rest-frame optical at the mean redshift of the first 3 bins, but shifts to the rest-frame violet/near-UV (3700 Å to 3290 Å) in the last bin ($z \sim 0.6$ to 0.8). Galaxies tend to look slightly more asymmetric at near-UV wavelengths due to the prominence of young stars. Thus, it is important to quantitatively test the the impact of bandpass shift on our visual classes. For this test, we use the redder F850LP images from the GOODS survey, which overlaps with the central 20% of the GEMS survey area. The F850LP filter has a pivot wavelength of 9103 Å and traces the rest-frame optical (7340 Å to 5057 Å) in all four redshift bins out to $z \sim 0.8$. They also have 5 times longer exposures than the GEMS F850LP and F606W images. Fig 5 shows GEMS F606W and GOODS F850LP images of typical disturbed and normal galaxies in the last 2 redshift bins ($z \sim 0.47$ to 0.8). While the GOODS images have higher S/N, and trace somewhat redder older stars, they do not reveal dramatically different morphologies from from those in the GEMS F606W images (Fig 5). Furthermore, the 855 intermediate mass ($M \geq 1 \times 10^9\ M_{\odot}$) galaxies in the GEMS/GOODS overlap area, were classified using both GOODS F850LP and GEMS F606W images by the 3 classifiers. We find that the ratio of ($f_{\rm GEMS}/f_{\rm GOODS}$) ranges from 0.9 to 1.2 across the 3 classifiers, where $f_{\rm GEMS}$ and $f_{\rm GOODS}$ are the fraction of strongly interacting ('Int') galaxies based on the GEMS F606W and GOODS F850LP images, respectively. In effect, over 85% of the galaxies classified as disturbed ('Int') in the GEMS F606W images retain the same visual class in the GOODS F850LP. Among the remaining objects, some classified as 'Normal' in GEMS F606W get reclassified as disturbed in GOODS F850LP, and vice-versa The fact that f does not change by a large amount between GEMS

F606W and GOODS F850LP is not surprising, since the rest-frame wavelength of GEMS F606W in the last bin shifts only to the violet/near-UV, rather than to the far-UV, where morphological changes are more dramatic. We conclude that our results are not highly impacted by bandpass shifting, and any effect is accounted for by our error bars of $> 30\%$ in f.

Another redshift-dependent systematic effect is surface brightness dimming at the rate of $(1+z)^{-4}$ (e.g., Barden et al. 2007). This leads to surface brightness dimming by a factor of 1.0 to 2.5 magnitude over the redshift range 0.24 to 0.80. This is mitigated in part by two factors: galaxies are on average 1.0 magnitude brighter in surface brightness by $z \sim 0.8$ (e.g., Barden et al. 2005), and the average SFR rises by a factor of ~ 4 out to $z \sim 0.8$ (e.g., see § 4.6). Two approaches can be adopted to assess the impact of surface brightness dimming. The first is to artificially redshift strongly disturbed galaxies in the lowest redshift bin ($z \sim 0.24$) out to $z \sim 0.8$, either assuming passive evolution or adding in a ~ 1 magnitude of brightening in surface brightness. Examples using the FERENGI code are shown in Fig 6. However, this approach suffers from the limitation that it implicitly assumes that galaxies at $z \sim 0.8$ are similar to those at $z \sim 0.24$ and evolve passively with time. A better approach, which does not make such assumptions, is to repeat the analysis and visual classification using *deeper* images of the galaxies and assess the resulting change in visual classes. The above-described test performed using the deep GOODS F850LP image (Fig. 5) is an example of such a test.

Finally, we checked the distribution of Sérsic indices n for single-component Sérsic fits (Barden et al. 2005) for the visual classes of the sample S2 of 3860 galaxies with $M \geq 1 \times 10^9$ $M_\odot$ (Fig. 7). Non-interacting disk-dominated systems are expected to have $n < 2.5$, while massive ellipticals and bulge-dominated systems typically have higher Sérsic indices. We indeed find that over 85% of the systems visually classified as Sb-Sd and Irr have $n < 2.5$ in the intermediate mass ($M \geq 1 \times 10^9$ $M_\odot$) sample. The systems typed as ellipticals (E) have mostly $n > 3$, and as expected, their distribution peaks at $n \sim 4$, corresponding to a de Vaucouleurs profile. The S0 and Sa types have n values bridging those of the E and disk (Sb-Sc and Sd-Irr) systems. Most of them have $n < 3$, but there is a long tail of S0s and Sas with higher n. This is expected given the previously described (§ 3.2) difficulties in separating E, S0, and Sa galaxies at intermediate redshifts. However, this ambiguity between Es, S0s and Sas is not a problem for the subsequent analyses in this paper, since galaxies are grouped together either as 'E+S0+Sa' or 'E-to-Sd'. In fact, as stressed in § 3.2, the main results presented in this paper depend only on the differences between three groups: strongly interacting galaxies ('Int') and non-interacting galaxies, divided between 'E to Sd' and 'Irr'.

4.2. Tests on the interaction fraction from CAS

In numerous published studies, the CAS merger criterion ($A > 0.35$ and $A > S$) is widely used, in a blind automated mode, to identify strongly interacting galaxies. However, few systematic studies have been done of the potential caveats, which include the following: a) The CAS criterion ($A > 0.35$ and $A > S$) will miss out strongly interacting galaxies where the morphological distortions contribute to more than 35 % of the total galaxy flux. (b) Calibrations of A with N-body simulations (Conselice 2006) shows that during major mergers with mass ratios 1:1 to 1:3, the asymmetry oscillates with time. Typically, it exceeds 0.35 for $\sim$ 0.2 Gyr in the early phases when the galaxies start to interact, falls to low values as the galaxies separate, rises for $\sim$ 0.2 Gyr as they approach again for the final merger, and eventually tapers down as the final remnant relaxes. On average, the $A > 0.35$ criterion is only satisfied for one third of the merger timescale in these N-body simulations. For minor mergers of mass ratios 1:5 and below, the asymmetries are too low to satisfy $A > 0.35$. (c) To complicate matters, automated asymmetry parameters can also capture non-interacting galaxies whose visible light shows small-scale asymmetries due to star formation (e.g., Miller et al. 2008)

We assess the effectiveness of the CAS merger criterion ($A > 0.35$ and $A > S$) for our dataset in several ways. The CAS asymmetry A and clumpiness S parameter are plotted for galaxies in the four bins covering the redshift interval $z \sim 0.24$–0.80 (Fig. 8). Galaxies satisfying the CAS criterion lie in the upper left hand corner, bracketed by the $A = S$ and $A = 0.35$ lines. One can see that while the CAS criterion captures a fair fraction of the strongly interacting galaxies (coded as orange stars), it also picks up a large number of normal non-interacting galaxies.

The top panel of Fig. 9 show the recovery fraction of CAS, defined as the fraction of the visually-classified strongly interacting galaxies ('Int') picked up by the CAS criterion ($A > 0.35$ and $A > S$). For the intermediate mass ($M \geq 1 \times 10^9$ $M_\odot$) sample, the CAS criterion picks up only 40% to 50% of the galaxies visually typed as strongly interacting ('Int'). We inspected the systems missed out by the CAS criterion ($A > 0.35$ and $A > S$) and show typical cases in Fig. 10. They include galaxies with tidal features and debris (e.g., light bridges between galaxies, tidal tails, arcs, shells, small accreted satellite in the main disk of a galaxy), which likely contribute less than 35% of the total light (e.g., cases 1 and 3 in Fig. 10). In addition, in galaxies with close double nuclei where the center is assumed to be between the two nuclei, the resulting low A will prevent the system from satisfying the CAS criterion (e.g., case 2 in Fig. 10).

The lower panel of Fig. 9 illustrates the contamination level of the CAS system. $N_{\rm CAS}$ represents the number of systems picked up by the CAS criterion ($A > 0.35$ and $A > S$)

in the four redshift bins. The vast majority (65% to 85%) of these systems turn out to be non-interacting 'Normal' galaxies of type 'Irr', and 'Sb-Sd'. Typical cases are shown in Fig. 10. They include the following: non-interacting actively star-forming systems where SF induces small-scale asymmetries in the optical blue light (e.g., cases 4 and 6 in Fig. 10); systems where A is high due to the absence of a center or due to the center being blocked by dust (e.g., cases 4 and 9 in Fig. 10); galaxies whose outer parts look irregular (e.g., cases 7 and 8 in Fig. 10); edge-on systems and compact systems, where the light profile is steep such that small centering inaccuracies can lead to large A (e.g., case 9 in Fig. 10).

Fig 4 compares the interaction fractions that would be obtained using the CAS criterion ($f_{\rm CAS}$), as opposed to visual classification (f). The visually based and CAS-based fractions agree within a factor of two, with f tending to be systematically higher than $f_{\rm CAS}$) at $z < 0.5$ and lower at $z > 0.5$. However, we caution that the systems counting toward $f_{\rm CAS}$ are a mixed bag, since the CAS criterion misses about half of the visually-classified strongly interacting galaxies (Fig. 9, top panel), but picks up a significant number of non-interacting dusty, star-forming galaxies (Fig. 9, lower panel). This contamination will affect the integrated properties of interacting systems captured by CAS and these caveats must be borne in mind in studies that use CAS in blind automated mode.

4.3. Interaction history of massive galaxies

Based on the tests in § 4.1 and § 4.2, we decide to adopt the mean interaction fraction f based on visual classes, with a conservative error bar that includes the sum in quadrature of the binomial deviation σ, the dispersion of ± 30% between classifiers, and an extra factor of ± 20% (tbc) due to bandpass shift and surface brightness dimming effects. The resulting interaction fraction f among high mass ($M \geq 2.5 \times 10^{10}\ M_{\odot}$) galaxies is shown in Fig. 12 and Table 1.

We conclude that the fraction f of strongly interacting systems among high mass ($M \geq 2.5 \times 10^{10}\ M_{\odot}$) galaxies varies from 6% ± 2% to 12% ± 4% over $z \sim 0.24$–0.80 (lookback time ∼ 3–7 Gyr), as averaged over every Gyr bin. As discussed in § 3.1, these systems are candidates for a recent/ongoing interaction of mass ratio $M1/M2 > 1/10$. Simulations suggest that the visibility timescale ($t_{\rm vis}$) over which strong morphological distortions can be identified ranges from 0.2 to 0.5 Gyr, depending on the gas mass fraction and mass ratio (e.g., Cox et al. in prep.). For an assumed visibility timescale of ∼ 0.3 Gyr, our distortion fraction f implies that *each massive galaxy has undergone at least 1.3 interactions of mass ratio > 1/10 since $z \sim 0.80$.* Thus, our results suggest that interactions of mass ratio > 1/10 are prevalent over the last 7 Gyr, albeit at lower frequency than at $z > 2$, where

a larger fraction ($f > 40\%$) is reported (e.g., Conselice 2003).

There are numerous astrophysical questions for which it would be useful to know which of these systems are major ($M1/M2 \geq 1/4$) versus minor ($1/10 \leq M1/M2 < 1/4$) interactions. However, the morphological distortions induced in an interaction depend not only on the mass ratio $M1/M2$ of the progenitors, but also on the orbital geometry (prograde or retrograde), the gas mass fraction, and structural parameters (e.g., Mihos & Hernquist 96; Struck 1997; Naab & Burkert 2001; Mihos et al. 1995, di Matteo et al. 2007). For instance, both types of mergers can cause strong tidal disturbances, drive large gas inflows into the inner kpc and trigger intense starbursts or AGN activity (e.g, review by Jogee 2006 and references therein). Furthermore, prograde mergers occur faster than retrograde mergers, lead to more violent disruption, and excite larger non-circular motions (e.g., Binney & Tremaine 1987). Thus, we assign the class 'major or minor interaction' to many strongly interacting galaxies where we cannot translate the morphological distortions into a unique mass ratio $M1/M2$. These include the following cases: a) Galaxies with double nuclei that are asymmetrically located, have different luminosities, and whose mass ratio is unknown as the system has only one single stellar mass based on COMBO-17 data (e.g., case 9 in Fig. 2). b) Systems with a morphological distortion that is strong, but not a 'train-wreck' (e.g., cases 4 and 14 in Fig. 2).

However, for a subset of the strongly interacting ('Int') galaxies, we can use stellar masses and unique morphological tell-tale signatures to make a fairly reliable distinction between the two types of interaction, and thus to set *a lower limit* to the frequency of major and minor interactions. We assign a class of 'minor interaction' to the following cases: (a) We consider galaxies that have undergone a recent interaction, but still host an extended disk to be a case minor merger, since such mergers do not destroy disks. We include in this group isolated galaxies that harbor a warped disk or strongly distorted disk with tidal debris, but are in a post-interaction phase, as indicated by the absence of another massive interacting companion with the same spectrophotometric redshift (e.g., cases 2, 3, 7, 8, 11, 12, 13, and 15 in Fig. 2). (b) We include galaxies (see § 3.2) with a companion that satisfies three criteria: it is overlapping or in contact so that the two galaxies share a common envelope of light; it has the same Combo-17 spectrophotometric redshift within the accuracy $\delta_z/(1 + z) \sim 0.02$ (§ 2); and its stellar mass ratio satisfies ($1/10 \leq M1/M2 < 1/4$). Such minor mergers are in progress (e.g., case 10 in Fig. 2).

We assign a class of 'major interaction' to the following cases: (a) Galaxies with extremely distorted 'train-wreck' morphologies (e.g., case 1 in Fig. 2). (b) Galaxies with double nuclei that are symmetrically located and have comparable luminosities (e.g., case 5 in Fig. 2). (c) Galaxies with a companion that satisfies three criteria: it is overlapping or in

contact so that the two galaxies share a common envelope of light; it has the same Combo-17 spectrophotometric redshift within the accuracy $\delta_z/(1+z) \sim 0.02$ (§ 2); and its stellar mass ratio satisfies ($1/10 \leq M1/M2 < 1/4$). Such major mergers are in progress (e.g., cases 1, 6, 16 in Fig. 2).

From the above analyses, the classes 'minor interaction', 'major interaction', and 'major or minor interaction', are assigned to $\sim 45\%$, $\sim 25\%$, and $\sim 30\%$, respectively of the strongly interacting galaxies. This implies the fraction of high mass galaxies undergoing a minor and major interaction is, $f_{\rm minor} \geq 4.5\%$ and $f_{\rm major} \geq 2.5\%$, respectively. Again, for an assumed visibility timescale of ~ 0.3 Gyr, this distortion fraction implies that *each massive galaxy has undergone at least 0.33 major and 0.60 minor interactions since $z \sim 0.80$.* To our knowledge, this is the first direct empirical estimate of the frequency of minor mergers over the last 7 Gyr, since $z \sim 0.80$. It provides an important constraint since minor mergers dominate the merger rates in LCDM models at $z < 1$.

4.4. Comparison with other studies

It is not straightforward to compare our observed fraction f of strongly interacting ('Int') galaxies in the high mass ($M \geq 2.5 \times 10^{10}\ M_\odot$) sample over $z \sim 0.24$–0.80 with published studies for several reasons. Many studies have small samples and large error bars at $z < 0.8$ (e.g., Conselice 2003; Fig. 11). Others focus on bright galaxies and luminosity-selected samples (e.g., Lotz et al. 2008; Casato et al. 2005) rather than stellar mass selected sample, because the data to derive stellar masses were unavailable. Different studies target different systems, ranging from morphologically distorted galaxies to close pairs with separation $d \sim 5$ to 30 kpc. Finally, most studies focus only on major interactions, while the strongly interacting galaxies identified in our study are candidates for a recent/ongoing interaction of mass ratio $M1/M2 > 1/10$ (§ 3.1), and include both minor and major interactions. Nonetheless, we attempt approximate comparisons.

Fig. 11 shows the the fraction $f_{\rm Gini}$ of morphologically disturbed systems based on Gini-M20 parameters among $M_{\rm B} <$ -20.5 and $L_{\rm B} > 0.4\ L_*$ galaxies in the Extended Groth Strip (Lotz et al. (2008). The latter study does not present any results for a high mass sample, and thus we effectively are comparing their bright galaxies to our high mass galaxies. Over $z \sim$0.2–0.60, our results are in very good agreement with $f_{\rm Gini}$. Over $z \sim$0.80–1.2, there is less good agreement, but the deviation from f is a factor of less than two. The CAS-based results from Conselice (2003) are derived from a small sample in the Hubble Deep Field and have error bars that are too large to set useful constraints at $z < 1$ (Fig. 11).

The major merger fraction of massive galaxies ($M_* \geq 2.5\times10^{10}\ M_\odot$) in close ($d < 30$ kpc) pairs based on the 2-point correlation function, is 5% ± 1% averaged over at $0.4 < z < 0.8$ (Bell et al. 2007). The study of luminous ($L_V > 0.4\ L_*$) pairs at projected separations of 5–20 kpc in the COSMOS field (Kartaltepe et al. 2007) finds a galaxy pair fraction of ∼ 1%–3% over $z \sim 0.24$–0.80, corresponding to a galaxy merger fraction of ∼ 2%–6% (Fig. 11). Our observed fraction f of ∼ 6% to 12% over $z \sim 0.24$–0.8, and our lower limit on the major merger fraction ($f_{\rm major} \geq 2.5\%$) bracket these results. The merger fraction based on close pairs seems to more closely trace the major merger fraction $f_{\rm major}$ from our studies, rather than the total f, as might be expected. However, one should note the following caveats in this comparison. The merger fraction based on close pairs depends on the correction applied to the projected close pair fraction to account for contamination from false pairs caused by chance line-of-sight projection. The correction is model-dependent and depends on the detailed form of the correlation function and uncertainties in the photometric redshifts (e.g., Bell et al. 2007; Kartaltepe et al. 2007). Furthermore, even pairs with members at the same redshift may not be gravitationally bound, and may therefore not evolve into a strong interaction or merger in the future. These factors may cause this method to overestimate the major merger fraction. Another complication when comparing pair-based fraction to our results is that strongly interacting galaxies (as defined in § 3.2) trace a later phase of interaction than the early pre-merger phases traced by close pairs.

4.5. Comparison of interaction history with LCDM simulations

Before comparing our empirical constraints on the interaction history of galaxies to predictions from different ΛCDM-based simulations of galaxy evolution, it is useful to recapitulate our results. We found that the fraction f of strongly interacting systems among high mass ($M \geq 2.5 \times 10^{10}\ M_\odot$) galaxies varies from 6% ± 2% to 12% ± 4% over $z \sim 0.24$–0.80 (lookback time ∼ 3–7 Gyr), as averaged over every Gyr bin (Fig. 12). The systems are candidates for a recent/ongoing interaction of mass ratio $M1/M2 > 1/10$. The fraction of high mass galaxies undergoing a minor ($1/10 \leq M1/M2 < 1/4$) and major ($M1/M2 \geq 1/4$) interaction are $f_{\rm minor} \geq 4.5\%$ and $f_{\rm major} \geq 2.5\%$, respectively. For an assumed visibility timescale of ∼ 0.3 Gyr, our results imply that each massive galaxy has undergone at least 1.3 interactions of mass ratio $> 1/10$ since $z \sim 0.80$, with at least 0.33 major and 0.60 minor interactions. The galaxy interaction rate R per unit co-moving volume per Gyr is a few $\times10^{-4}$ galaxies Gyr^{-1} Mpc^{-3} (Fig. 13), based on $R = (nf/t_{\rm vis})$, where n is the comoving number density of galaxies in the mass range of interest.

We first discuss comparisons with the semi-analytical models of Somerville et al. (in

prep.), and Benson et al. (2005). In semi-analytical models, approximate or simplified treatments are used to model merger timescales, star formation, feedback, and the conversion of disk into spheroids (e.g., Somerville et al. in prep.; Benson et al. 2005; Somerville & Primack 1999; Cole et al. 2000). The dark matter halo merger history is set from the cosmological power spectrum, while the baryonic merger history depends on the input baryonic physics and halo occupation statistics. For the model of Somerville et al. (in prep.), AGN feedback is included and it controls the baryonic accretion history, thus shaping the associated mass function (MF) of galaxies. Normalization is carried out using the local COMB0-17 constraints. The merger rate R in the simulation box is determined by tracing the merger history and recording the time at which the galaxy had its last major ($M1/M2 \geq 1/4$) or minor ($1/10 \leq M1/M2 < 1/4$) merger. The merger fraction f is determined from mock catalogs based on the simulations.

For the models of Hopkins et al. (2007), cosmological halos and sub-halos are populated with galaxies following an empirical halo occupation model, which is constrained to match the clustering as a function of mass and mass functions of red/blue galaxies. When halos/sub-halos merge, the galaxy merger rate can be calculated via standard or modified dynamical friction formulae. Some of the modified formulae include a gravitational capture cross section, allow for stripping of halos or calibration with N-body simulations. Depending on the models adopted for sub-halo structure and mass functions, the halo occupation statistics, and the dynamical friction formulae used, the model predictions can vary by a factor of order two. AGN feedback is included.

Within a factor of $\sim$ 2–3, we find good agreement for f (Fig. 12) and R (Fig. 13 between the data and predictions for (minor + major) mergers (solid lines) from the semi-analytical models of Somerville et al. (in prep.; marked as 'S'), HOD models of Hopkins et al. (2007; marked as 'H'). This is rather remarkable given all the uncertainties involved in the model prescriptions of the baryonic merger history. Separate comparisons with the major merger or minor merger fraction is more difficult as we only have lower limits.

Next we consider cosmological hydrodynamic simulations. These attempt to incorporate the detailed physics of gas hydrodynamics, gravitational interactions, star formation, feedback and include the effect of the large-scale environment (e.g., Maller et al. 2006; Navarro & Steinmetz 2000; Robertson et al. 2004; Governato et al. 2004). However, they often do not have the dynamic range to resolve galaxies over a significant mass range while simultaneously modeling representative cosmological volumes. We first show results from the smoothed particle hydrodynamics (SPH) cosmological simulations of Maller et al. (2006). The simulation box is $22.2h^{-1}$Mpc on a side, and has a spatial resolution of 5 h^{-1}kpc, with the dark matter and gas components modeled with $(128)^3$ particles each. No AGN feedback

is included. The fraction and rate R of major merger (defined here as $1/3 \leq M1/M2 < 1/1$) among $3.0 \times 10^{10} < M_*/M_\odot < 2.2 \times 10^{11}$ are shown in Fig. 12 and Fig. 13 (marked as 'M'). The limited dynamic range of the current simulations does not allow any predictions for minor mergers. We first note that while the major merger fraction f of Maller et al (2006) shows fair agreement with other models (Fig. 12), the merger rate R is *a factor of 30 to 60 lower* than those of Somerville et al. (in prep) and HOD models of Hopkins et al. (2007) on Fig. 13. The major merger rate R is also *a factor of 30* lower than our empirical lower limit of 5×10^{-5} galaxies Gyr^{-1} Mpc^{-3} (Fig. 13). While uncertainties of a factor of a few exist in the visibility timescale ($t_{\rm vis}$) of morphological distortions, they cannot account for a such a large discrepancy between data and model or between models. The discrepancy must be largely due to the difference in the galaxy mass function of the SPH simulations and semi-analytic models. In particular, it may be due to an over-prediction in the relative number of high mass galaxies, caused by the *the lack of AGN feedback or other mechanism to shut off baryonic accretion* in the SPH models.

We also show results from the Millennium Run, the largest simulation to date of structure formation within a ΛCDM cosmogony. The run uses 10^{10} particles to follow the dark matter distribution in a cubic region $500h^{-1}$Mpc on a side, and has a spatial resolution of 5 h^{-1}kpc. [NB: I am waiting for Volker Springel's values on this, with or w/o AGN feedback].

[NB: After the Fig. 12 and Fig. 13 were made and shown in Rome, the N-body simulations of Donghia et al. (2008) appeared from the Zurich group. There have just been added on the figures and is marked as 'D'. I am awaiting their paper to add the technical description and assumptions of their simulations].

4.6. The impact of galaxy interactions on the average SFR over the last 7 Gyr

The impact of galaxy interactions on the cosmic SF history of galaxies is of great astrophysical interest. The idea that galaxy interactions enhance the SFR of galaxies and trigger strong nuclear starbursts is well established from observations (e.g. Larson & Tinsley 1978; Joseph & Wright 1985; Kennicutt et al. 1987; Barton et al 2003) and simulations (e.g., Negroponte & White 1983; Hernquist 1989; Barnes & Hernquist 1991, 1996; Mihos & Hernquist 1994, 1996; Barnes 2004; Springel, Di Matteo & Hernquist 2005). However, simulations cannot robustly predict the impact of galaxy interactions on the SF activity of galaxies over the last 7 Gyr, since both the SFR and properties of the remnants in simulations are highly sensitive to the stellar feedback model, the bulge-to-disk (B/D) ratio, the gas mass fractions, and orbital geometry (e.g., Cox et al 2006; di Matteo et al. 2007).

We adopt the SFRs in Bell et al. (2005, 2007), based on Combo-17 UV data (Wolf et al. 2004) and deep Spitzer 24 μm observations with a limiting flux of $\sim$ 83 μ Jy from the Spitzer Guaranteed Time Observers (Papovich et al. 2004; Gordon et al. 2005). The unobscured SFR based on the directly observable UV light from young stars was computed using $\mathrm{SFR_{UV}} = 9.8 \times 10^{-11}$ (2.2 L_{UV}), where $L_{\mathrm{UV}} = 1.5 \nu l_{\nu,2800}$ is a rough estimate of the total integrated 1216–3000 Å UV luminosity, derived using the 2800 Å rest-frame luminosity from COMBO-17 $l_{\nu,2800}$. The factor of 1.5 used in converting the 2800 Å luminosity to total UV luminosity accounts for the UV spectral shape of a 100 Myr-old population with constant SFR. The factor of 2.2 corrects for the light emitted longward of 3000 Å and shortward of 1216 Å. The SFR calibration is derived from Pégase assuming a 100 Myr old stellar population with constant SFR and a Chabrier (2003) IMF. The obscured SFR can be calculated from dust-reprocessed IR emission using the expression $\mathrm{SFR_{IR}} = 9.8 \times 10^{-11}$ L_{IR}, where L_{IR} is the total IR luminosity (TIR) over 8–1000 μm. L_{IR} is constructed from the observed 24 μm flux (corresponding to rest-frame wavelengths of 19–13 μm over $z \sim 0.24$–0.80) using the method outlined in Papovich & Bell (2002), based on an average Sbc template from the Devriendt et al. (1999) SED library. In converting from L_{IR} to $\mathrm{SFR_{TIR}}$, Bell et al. (2007) assume that the bulk of the 24 μm emission comes from SF, and not from AGN activity, based on the statistical result that less than 15% of the total 24 μm emission at $z < 1$ is in X-ray luminous AGN (e.g., Silva et al. 2004; Bell et al. 2005; Franceschini et al. 2005; Brand et al. 2006). Uncertainties in these SFR estimates are no less than a factor of 2 for individual galaxies while the systematic uncertainty in the overall SFR scale is likely to be less than a factor of 2 (Bell et al. 2007).

The UV-based SFR is plotted *versus* the stellar mass in each redshift bin (Fig. 16). We investigate the SF properties of the sample S2 of 3860 galaxies with $M \geq 1.0 \times 10^9$ $M_{\odot}$. This sample is complete for the blue cloud, but incomplete for the red sequence in the highest redshift bins (§ 2). However, since most of the SFR density originates from the blue cloud, this incompleteness does not have any major impact on the results. The UV-based SFR ranges from $\sim$ 0.01 to 25 $M_{\odot}$ yr^{-1}, with most galaxies having a rate below 5 $M_{\odot}$ yr^{-1}. We are complete in the last bin down to $\sim$ 0.2 $M_{\odot}$ yr^{-1}. Only 23% of this sample ($\sim$ 900 galaxies) have a Spitzer 24 μm detection. They yield a median ratio of ($\mathrm{SFR_{IR}}/\mathrm{SFR_{UV}}$) of $\sim$ 3.6, indicative of a sustantial amount of obscured star formation. The average UV-based and UV+IR-based SFRs are plotted in Fig. 17. The value of $\mathrm{SFR_{UV+IR}}$ (Fig. 17; lower panel) in the first redshfit bin looks anomalously high compared to the corresponding $\mathrm{SFR_{UV}}$ (Fig. 17; top panel). We suspect that this is due to excess 24 μm emission from an AGN component. However, we do not attempt any correction because even this high $\mathrm{SFR_{UV+IR}}$ does not change the results below.

The fraction of strongly interacting galaxies is shown in Table . We find that over

$z \sim 0.24$–0.80 (lookback of 3 to 7 Gyr), the average UV-based and UV+IR-based SFR are only modestly enhanced in strongly interacting galaxies, compared to non-interacting galaxies (Fig. 17). Our results suggest that *over the last 7 Gyr since $z < 0.8$, the average SFRs of galaxies undergoing a strong interaction of mass ratio $M1/M2 > 1/10$ is not typically enhanced by an order of magnitude, but rather, suffer only a modest enhancement* (Fig. 17). This modest enhancement is consistent with the recent statistical study of di Matteo et al. (2007), who find from numerical simulations of several hundred galaxy collisions that that the maximum SFR in galaxy mergers is typically only a factor of 2-3 larger than that of corresponding normal non-interacting galaxies. Their results suggest that the results of some early simulations (e.g., Mihos & Hernquist 1996; Hernquist & Mihos 1995), where mergers converted 50 to 80 per cent of their original gas mass into stars, may not represent the typical situation at $z < 1$.

4.7. The contribution of interacting galaxies to the cosmic SFR density over the last 7 Gyr

Over the redshift interval $z \sim 0$ to 1, corresponding to the last 8 Gyr, the cosmic SFR density is claimed to decline by a factor of 3 to 10 (e.g., Madau et al. 1996, 1998; Cowie et al. 1996; Flores et al. 1999; Haarrsma et al. 2000). Here, we explore the relative contributions of interacting and non-interacting galaxies to the cosmic SFR density since $z < 1$.

For intermediate-to-high mass ($M \geq 1.0 \times 10^9\ M_\odot$) galaxies, we estimate the SFR density from strongly interacting and non-interacting galaxies over $z \sim 0.24$–0.80, using the UV-based and UV+IR-based SFR (Fig. 18). We find that *strongly interacting galaxies only account for a small fraction ($< 30\%$) of the cosmic SFR density over $z \sim 0.24$–0.80, corresponding to lookback times of 3–7 Gyr (Fig. 17).* Our results suggest, in fact, that the behavior of the cosmic SFR density over $z \sim 0.24$–0.80 is predominantly shaped by normal galaxies. Furthermore, our results agree remarkably well with models for the self-regulated growth of supermassive black holes in mergers involving gas-rich galaxies (Hopkins et al. 2005). These models predict that galaxy mergers contribute only $\sim 20\%$ of the SFR density of at $z \sim 1$, and even out out to $z \sim 2$. We note that our study extends earlier works, which reported that normal galaxies dominate the UV (Wolf et al. 2005) and IR (Bell et al. 2005) luminosity density over one redshift bin ($z \sim 0.65$–0.75), corresponding to lookback times of 6.2 to 6.8 Gyr. In contrast, our results over $z \sim 0.24$–0.80 correspond to lookback times of 3–7 Gyr, and extend by a factor of ~ 7 the time interval covered by earlier studies.

Do the results still hold given the uncertainties in identifying strongly interacting galaxies? In § 4.1, we have attempted to assess how the fraction f of strongly interacting galaxies

is impacted by various sources of uncertainties, such as the binomial standard deviation, the dispersion between classifiers, the effect of moderate bandpass shifting, and the effect of surface brightness dimming. The error bars on f of the order of $\pm 1.4 \times f$ already reflect these estimates and do not change the results that strongly interacting galaxies only account for a small fraction ($< 30\%$) of the cosmic SFR density over $z \sim 0.24$–0.80. We suggest two further tests: (1) Our non-interacting galaxies include two groups: 'E-to-Sd' and 'Irr' systems. In particular, we have operated under the assumption that galaxies, which host small-scale asymmetries that are likely caused by SF rather than interactions, should be considered as non-interacting systems and given the class 'non-interacting Irr' (§ 3.2). One may argue that there are a number of galaxies that would be borderline cases between interacting and non-interacting Irr. However, even in the extreme worst-case scenario where we would reclassify *all* the 'non-interacting Irr' as strongly interacting, our results would still hold, since the combined SFR density from the strongly interacting and 'non-interacting Irr' systems is still lower that of 'non-interacting E-to-Sd' systems. (2) Another test is to repeat the analyses using the CAS merger criterion ($A > 0.35$ and $A > S$) to identify strongly interacting galaxies. The limited recovery rate (40% to 50%) and significant contamination impacting the CAS criterion (§ 3.3) make it more difficult to interpret the SF properties of systems identified as strongly interacting ('CAS Dist') or non-interacting ('CAS Normal'). Nonetheless, it is reassuring that strongly interacting galaxies identified via the CAS criterion lead to the same conclusion on the average SFR (Fig. 19) and SFR density (Fig. 20) of strongly interacting galaxies, as compared to non-interacting galaxies.

For intermediate-to-high mass ($M \geq 1.0 \times 10^9\ M_\odot$) galaxies, we find that the cosmic SFR density declines by a factor of ~ 3 from $z \sim 0.80$ to 0.24 (lookback time ~ 7 to 3 Gyr). Since non-interacting galaxies dominate the cosmic SFR density in every redshift bin, it follows that this decline *is largely the result of a shutdown in the SF of relatively normal non-interacting galaxies.* The question of what drives this shutdown will be addressed in detail in paper II, and is only considered briefly here. One possibility is the depletion of the internal cold gas supply of galaxies by star formation, or the reduction in the accretion rate of gas from cosmological filaments. Future facilities like ALMA will be instrumental in exploring this issue further. Another related possibility is that over time, most of the SFR is shifting to lower stellar masses. This is illustrated in the dependence of the SFR (Fig. 16) and specific SFR (SSFR; Fig. 21) on stellar mass. High mass systems are associated with a lower SSFR (Fig. 21; see also Cowie et al. 1996; Brinchmann et al. 2004; Brinchmann & Ellis 2000; Fontana et al. 2003; Bauer et al. 2007), consistent with the idea that they have experienced the bulk of their stellar mass growth at earlier epochs ($z > 1$). In staged SF models (Noeske et al. 2007) the SF history of high (low) mass systems is consistent with exponential SF models associated with an early (late) onset and a short (long) duration.

5. Summary and Conclusions

We explore the frequency and impact of strong interactions on the star formation of galaxies over $z \sim 0.24$–0.80 (lookback times of 3–7 Gyr), based on *HST* ACS, COMBO-17, and Spitzer 24 μm data from the GEMS survey. Our approach complements existing studies in several ways: (1) We use a large sample of ~ 3800 ($M \geq 1 \times 10^9\ M_\odot$) galaxies and 800 high mass ($M \geq 2.5 \times 10^{10}\ M_\odot$) galaxies for robust number statistics (§ 2). (2) Two independent methods are used to identify strongly interacting galaxies: a tailored visual classification system complemented with spectrophotometric redshifts and stellar masses (§ 3.2), as well as the CAS merger criterion ($A > 0.35$ and $A > S$), based on CAS asymmetry A and clumpiness S parameters (§ 3.3). This allows the first systematic comparison to date between CAS-based and visual classification results (§ 4.2). We also try to assess the impact of moderate bandpass shifts and surface brightness dimming (§ 4.1). (3) We set up the visual classification system (§ 3.2) so as to target strong interactions with mass ratio $M1/M2 > 1/10$. While many earlier studies focused on major mergers, it is important to constrain minor mergers as well, since minor mergers dominate the merger rates in LCDM models at $z < 1$. Our results are:

1. Among $M \geq 1 \times 10^9\ M_\odot$ galaxies, the CAS criterion ($A > 0.35$ and $A > S$) picks only 40% to 50% of the galaxies visually-classified as strongly interacting galaxies, but picks up a large number of non-interacting dusty, star-forming galaxies. This contamination will affect the integrated properties of interacting systems captured by CAS and these caveats must be borne in mind in studies that use CAS in blind automated mode. (Fig. 8 and Fig. 9).

2. The observed fraction f of strongly interacting systems among $\sim$ 800 high mass ($M \geq 2.5 \times 10^{10}\ M_\odot$) galaxies varies from 6% $\pm$ 2% to 12% $\pm$ 4% over $z \sim 0.24$–0.80 (lookback time $\sim$ 3–7 Gyr), as averaged over every Gyr bin (Fig. 12). These systems are candidates for a recent/ongoing interaction of mass ratio $M1/M2 > 1/10$. The fraction f based on visual classes and CAS agree within a factor of two (Fig 4). For an assumed visibility timescale of ~ 0.3 Gyr, the results yield an interaction rate $R \sim$ a few $\times 10^{-4}$ galaxies Gyr^{-1} e.g., Mpc^{-3}, and imply that *each massive galaxy has undergone at least 1.3 interactions of mass ratio > 1/10 since $z \sim 0.80$.* Thus interactions of mass ratio $> 1/10$ are prevalent over the last 7 Gyr, albeit at lower frequency than at $z > 2$ where significantly larger f ($> 40\%$) are reported.

3. For a subset of the strongly interacting high mass galaxies, stellar masses and unique morphological tell-tale signatures enable us to decide whether the system is a major ($M1/M2 \geq 1/4$) or minor ($1/10 \leq M1/M2 < 1/4$) interaction. The resulting lower limit on the fraction of major and minor interactions is $f_{\rm minor} \geq 4.5\%$ and $f_{\rm major} \geq 2.5\%$,

respectively. For an assumed visibility timescale of ~ 0.3 Gyr, this distortion fraction implies that *each massive galaxy has undergone at least 0.33 major and 0.60 minor interactions since $z \sim 0.80$ (lookback time $\sim$ 7 Gyr).* To our knowledge, this is the first attempt to set observational constraints on the frequency of minor mergers over the last 7 Gyr.

4. We compare our results on the interaction history of high mass ($M \geq 2.5 \times 10^{10}$ $M_{\odot}$) galaxies to predictions from different ΛCDM-based simulations of galaxy evolution. To our knowledge, such extensive comparisons have not been attempted to date, and are long overdue. Within a factor of $\sim$ 2–3, we find good agreement for f (Fig. 12) and R (Fig. 13) between the data and the predictions for mergers of mass ratio $M1/M2 > 1/10$ from the semi-analytical models of Somerville et al. (in prep.) and HOD models of Hopkins et al. (2007). This is rather remarkable given all the uncertainties involved in the model prescriptions of the baryonic merger history. However, some cosmological SPH simulations without AGN feedback produce major merger rates that are a factor of 30-60 lower than the data or other models. We believe the disagreement is due to an over-prediction of high mass galaxies, which is likely caused by the lack of AGN feedback or other mechanism to shut off baryonic accretion in these simulations.

5. Among $M \geq 1.0 \times 10^{9}$ $M_{\odot}$ galaxies, we find that over $z \sim 0.24$–0.80, the UV-based and UV+IR-based average SFRs are only modestly enhanced in strongly interacting galaxies, compared to non-interacting galaxies (Fig. 17). Our results suggest that *over the last 7 Gyr, the average SFRs of galaxies undergoing a strong interaction of mass ratio $M1/M2 > 1/10$ do not typically get enhanced by an order of magnitude, but rather, suffer only a modest enhancement* (Fig. 17). This modest enhancement is consistent with the recent statistical study of di Matteo et al. (2007), who find from numerical simulations of several hundred galaxy collisions that that the maximum SFR in galaxy mergers is typically only a factor of 2-3 larger than that of corresponding normal non-interacting galaxies.

6. For intermediate-to-high mass ($M \geq 1.0 \times 10^{9}$ $M_{\odot}$) galaxies, our results of a modest interaction fraction f and a modest enhancement in SFR from interactions culminate in our finding that strongly interacting systems only account for a small fraction ($<$ 30%) of the cosmic SFR density over $z \sim 0.24$–0.80 (lookback time $\sim$ 3–7 Gyr; Fig. 17). In effect, contrary to common lore, our results suggest that *the behavior of the cosmic SFR density over the last 7 Gyr is predominantly shaped by normal non-interacting galaxies, rather than strongly interacting galaxies.* Our results are in good agreement with the SFR density predicted by models for the self-regulated growth of supermassive black holes in mergers involving gas-rich galaxies.

7. Over the redshift interval $z \sim 0$ to 1, corresponding to the last 8 Gyr, the cosmic SFR density is claimed to decline by a factor of 3 to 10 (e.g., Madau et al. 1996, 1998; Cowie et al. 1996; Flores et al. 1999; Haarrsma et al. 2000). For intermediate-to-high mass ($M \geq 1.0 \times 10^9\ M_\odot$) galaxies, we find that the cosmic SFR density declines by a factor of ~ 3 from $z \sim 0.80$ to 0.24. We suggest this decline is largely the result of a shutdown in the SF of relatively normal non-interacting galaxies. This shutdown may be driven by the depletion of the internal cold gas supply of galaxies, the reduction in the accretion rate of gas from cosmological filaments, and the transition of SF activity to lower stellar masses.

S.J. acknowledges support from the National Aeronautics and Space Administration (NASA) LTSA grant NAG5-13063, NSF grant AST-0607748, and *HST* grants GO-10395 and GO-10861 from STScI, which is operated by AURA, Inc., for NASA, under NAS5-26555. Support for GEMS was provided by NASA through *HST* grant GO-9500 CH acknowledges the support of a European Commission Programme 6$^{\rm th}$ framework Marie Cure Outgoing International Fellowship under contract M01F-CT-2006-21891. We thank Andrew Benson, Phil Hopkins, Ari Maller, and Andi Burkert, for useful discussions. This research has made use of NASA's Astrophysics Data System Service.

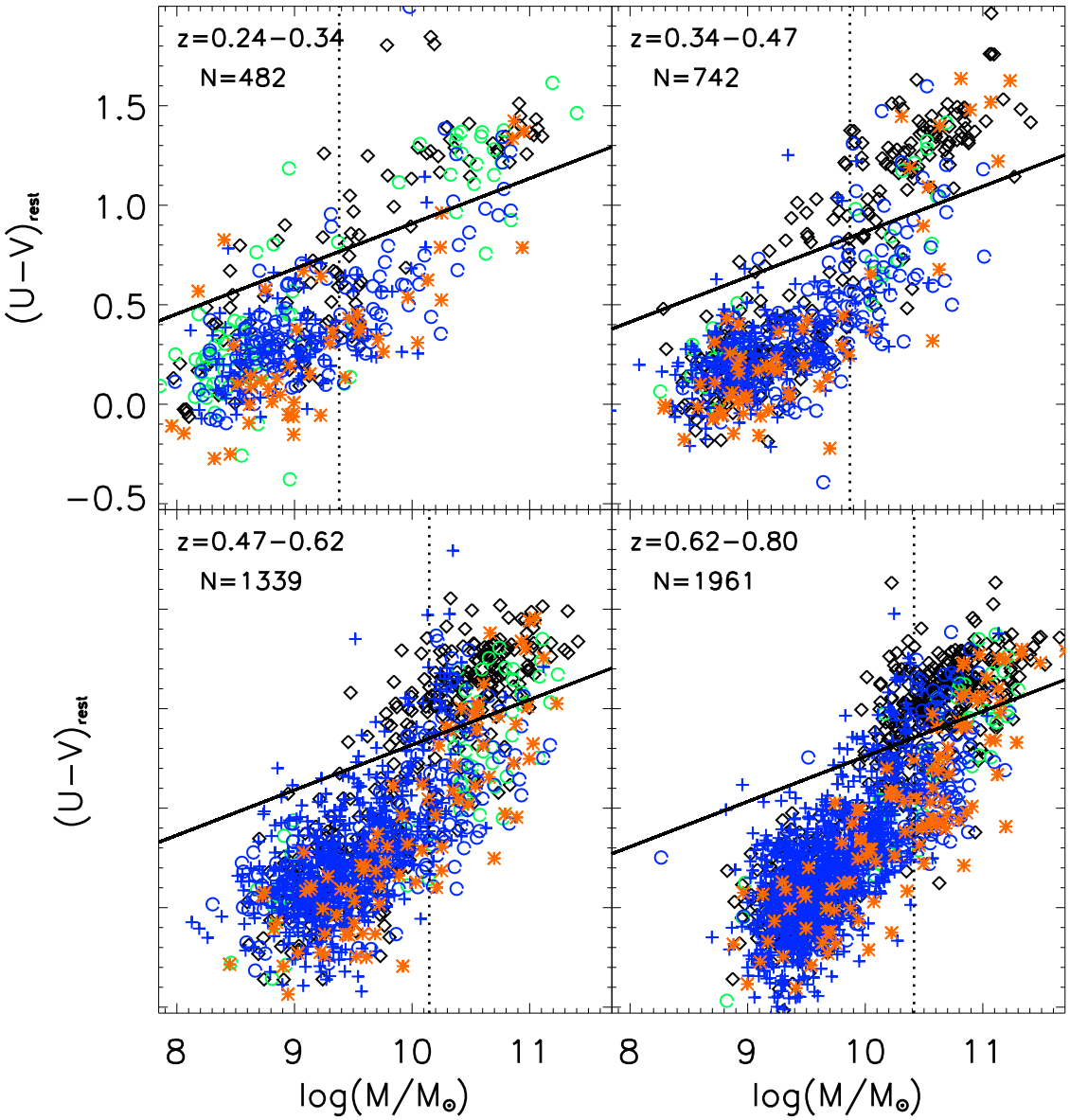

Fig. 1.— The rest-frame $U-V$ color is plotted *versus* the stellar mass in four redshift bins, which span 1 Gyr each, and cumulatively cover the interval $z \sim 0.24$–0.80 ($T_{\rm back} \sim 3$–7 Gyr). N denotes the number of galaxies in each bin. The diagonal line marks the separation of the red sequence galaxies and the blue cloud galaxies at the average redshift $z_{\rm ave}$ of the bin. The vertical lines marks the mass completeness limit (Borch et al. (2006) for the red sequence galaxies. The blue cloud galaxies are complete well below this mass. Galaxies are coded according to their visual type (VT) in the F606W band: strongly interacting systems (Dist; orange stars), and non-interacting E+S0 (black diamonds), Sa (green circles) Sb-Sc (blue circles) and Sd-Irr (blue crosses) galaxies.

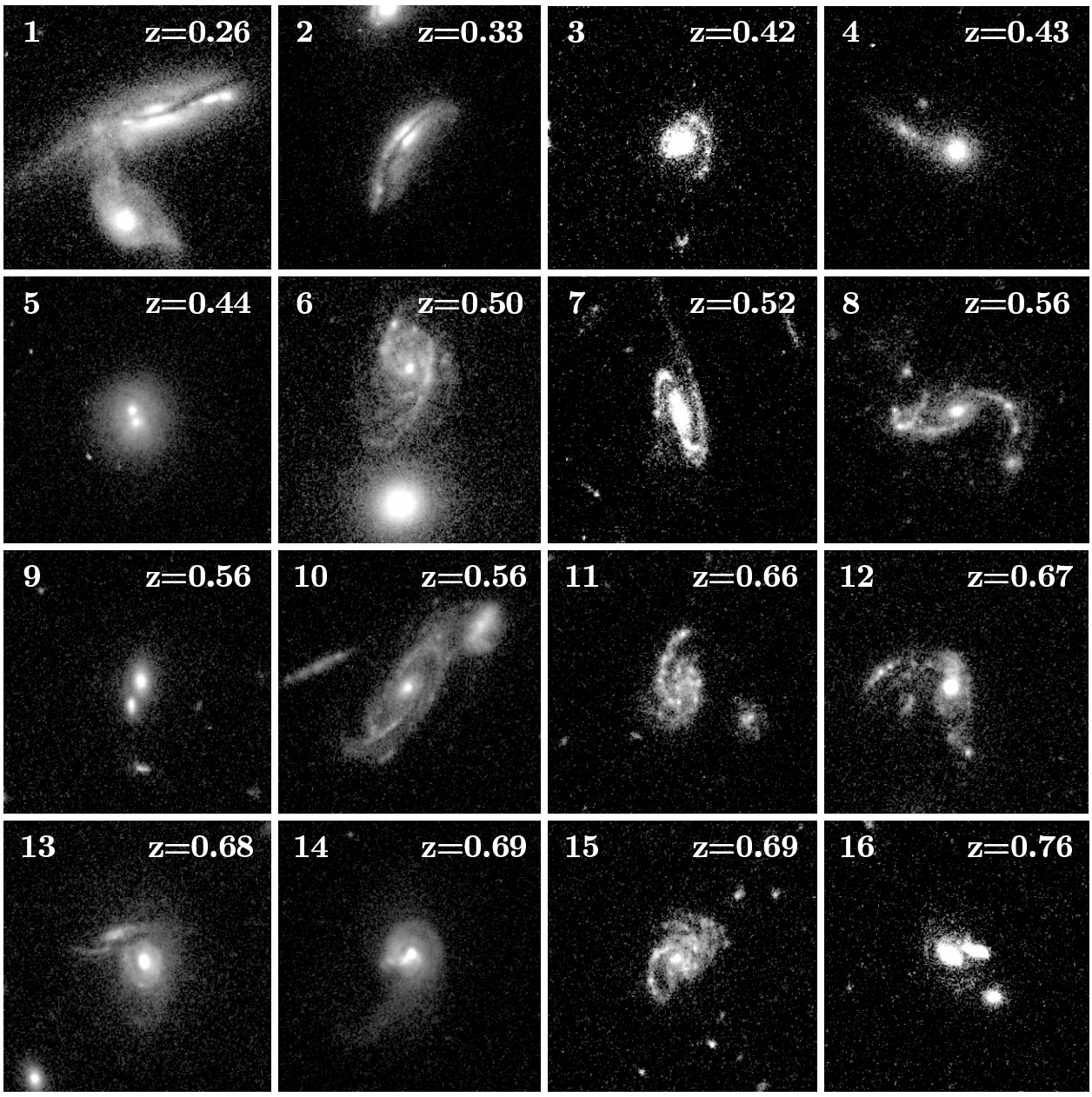

Fig. 2.— This montage show examples of high mass ($M \geq 2.5 \times 10^{10}\ M_{\odot}$) galaxies classified as strongly interacting (Dist) galaxies. These systems show strong morphological distortions, such as multiple nuclei or components connected by a bridge or common envelope (e.g., 1, 5, 6, 9, 10, 13, 16), warped disks (e.g., 2), and tidal tails, strongly asymmetric features, or accreting satellites (e.g., 3, 4, 7, 8, 11, 12, 14, 15). The strongly interacting galaxies are candidates for a recent/ongoing interaction of mass ratio $M1/M2 > 1/10$.

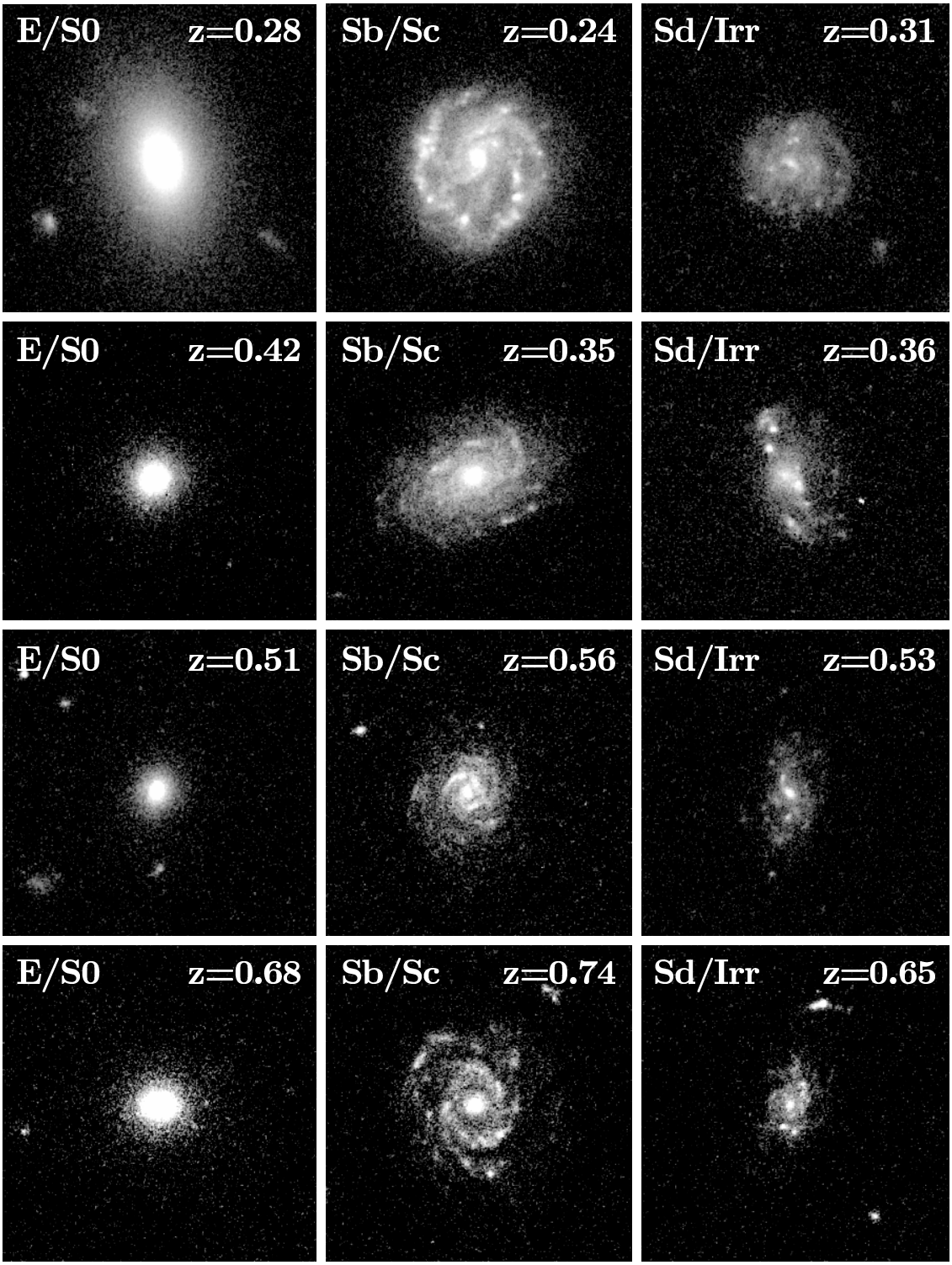

Fig. 3.— This montage shows examples of galaxies classified as non-interacting systems with visual types E/S0, Sb/Sc and Sd/Irr. The four rows show candidates from the four redshift bins in Figure 1.

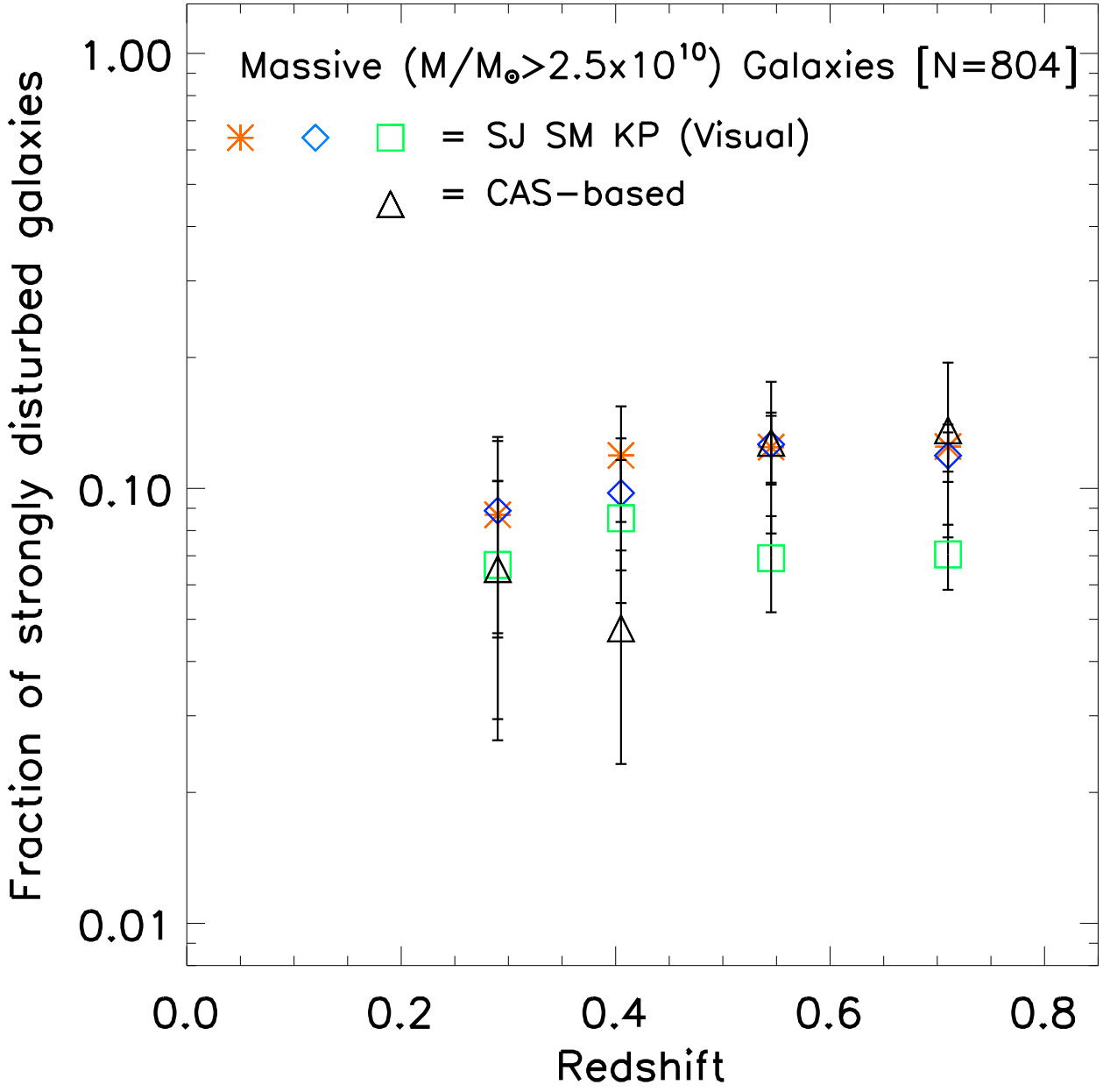

Fig. 4.— This figure compares the fraction ($f_{\rm VC}$) of strongly interacting galaxies, based on visual classification by three classifiers (SJ, SM, KP), as well the interaction fraction ($f_{\rm CAS}$) based on the CAS criterion ($A > S$ and $A > 0.35$). The error bar plotted for $f_{\rm VC}$ is based on the binomial standard deviation $\sigma = [N\ f_{\rm VC}(1\text{-}f_{\rm VC})]^{1/2}$ for each bin of size N. The dispersion between different visual classifiers is $\leq 30\%$ of $f_{\rm VC}$. The error bar for $f_{\rm CAS}$ is based on the errors on the asymmetry A parameters. The visually based and CAS-based interaction fraction agree within a factor of two. However, we caution that the systems counting toward $f_{\rm CAS}$ includes only 40% to 50% of the visually-classified strongly interacting galaxies (Fig. 9, top panel), and a large number of non-interacting dusty, star-forming galaxies (Fig. 9, lower panel).

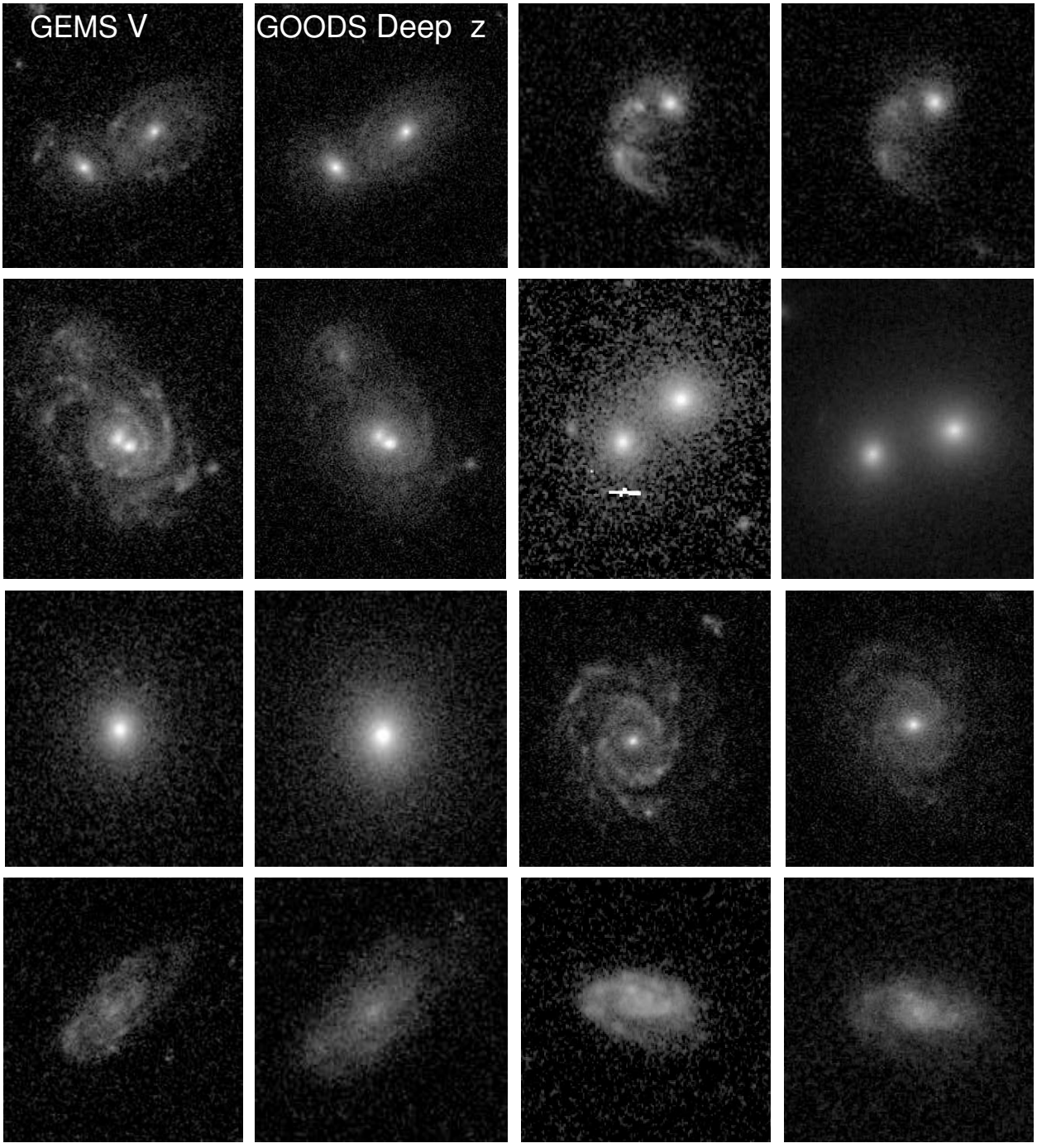

Fig. 5.— This montage illustrates a test for bandpass shift and surface brightness dimming. It shows GEMS F606W (V band; pivot $\lambda \sim 5915$ Å) and deep GOODS F850LP (z band; pivot $\lambda \sim 9103$ Å) images of typical strongly interacting and normal non-interacting galaxies in the last redshift bin ($z \sim 0.60$ to 0.80), where bandpass shift and surface brightness dimming are expected to be most severe. In this redshift bin, the rest-frame wavelength traced by the GEMS images shift from optical to violet/near-UV (3700 Å to 3290 Å). However, while the GOODS images trace the rest-frame optical and have higher S/N, the visual types assigned to the galaxies do not change. A statistical analysis is shown in Table 3.

Fig. 6.— Artificially redshifting of strongly interacting galaxies in the lowest redshift bin $z \sim 0.24$ out to $z \sim 0.8$ using FERENGI. We add in ~ 1 magnitude of brightening in surface brightness.

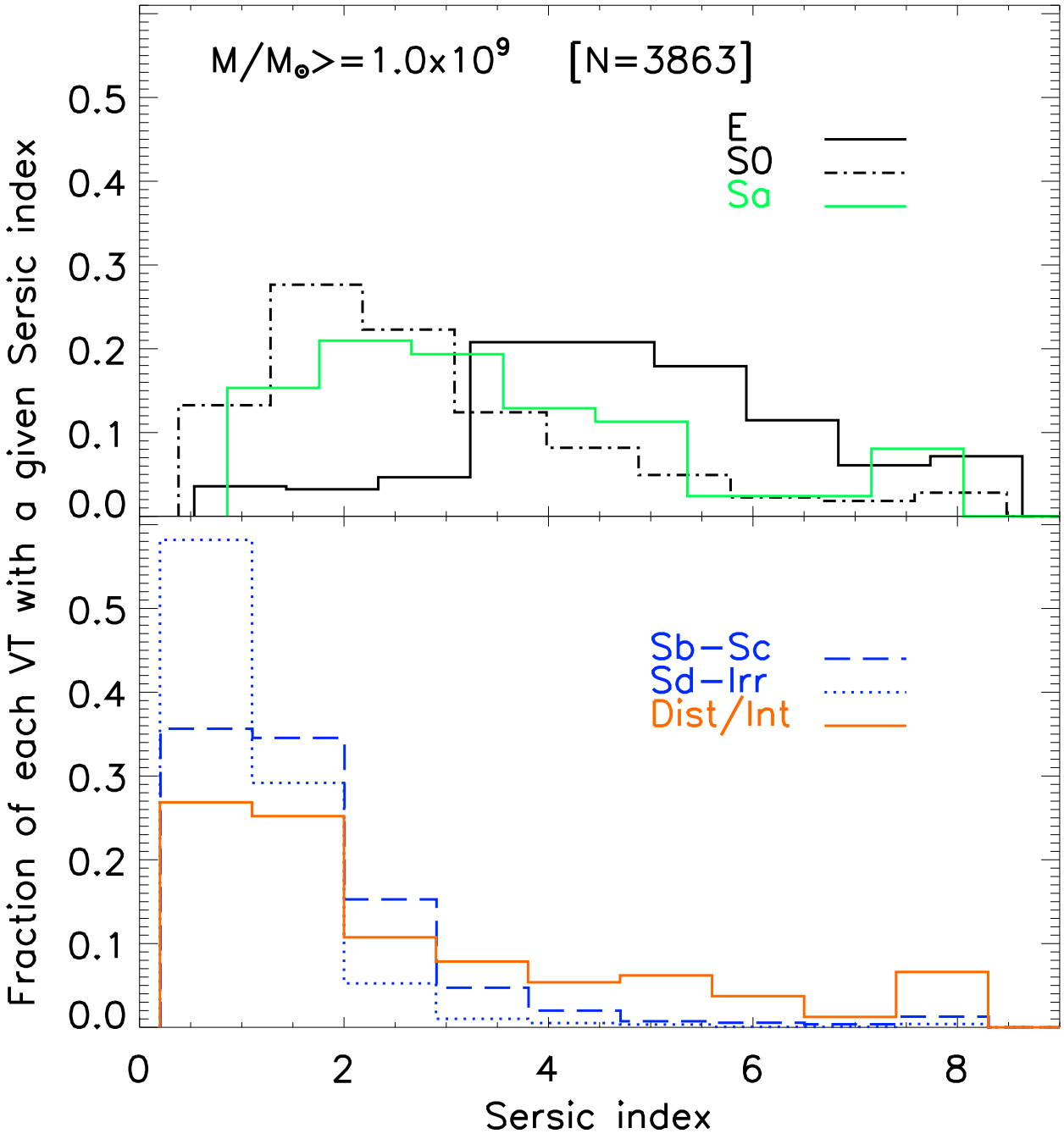

Fig. 7.— For intermediate mass ($M \geq 1 \times 10^9\ M_\odot$) galaxies, the distribution of Sérsic indices n from single-component Sérsic fits is plotted for non-interacting (E, S0, Sa, Sb-Sc, Sd-Irr) and strongly interacting (Dist) galaxies. The majority of systems visually classified as Sb-Sc and Sd-Irr have $n < 2.5$, as expected for disk-dominated systems. Most of the systems visually typed as E have $n > 3$ and their distribution peaks at $n \sim 4$, corresponding to a de Vaucouleurs profile. S0 and Sa systems have intermediate n values.

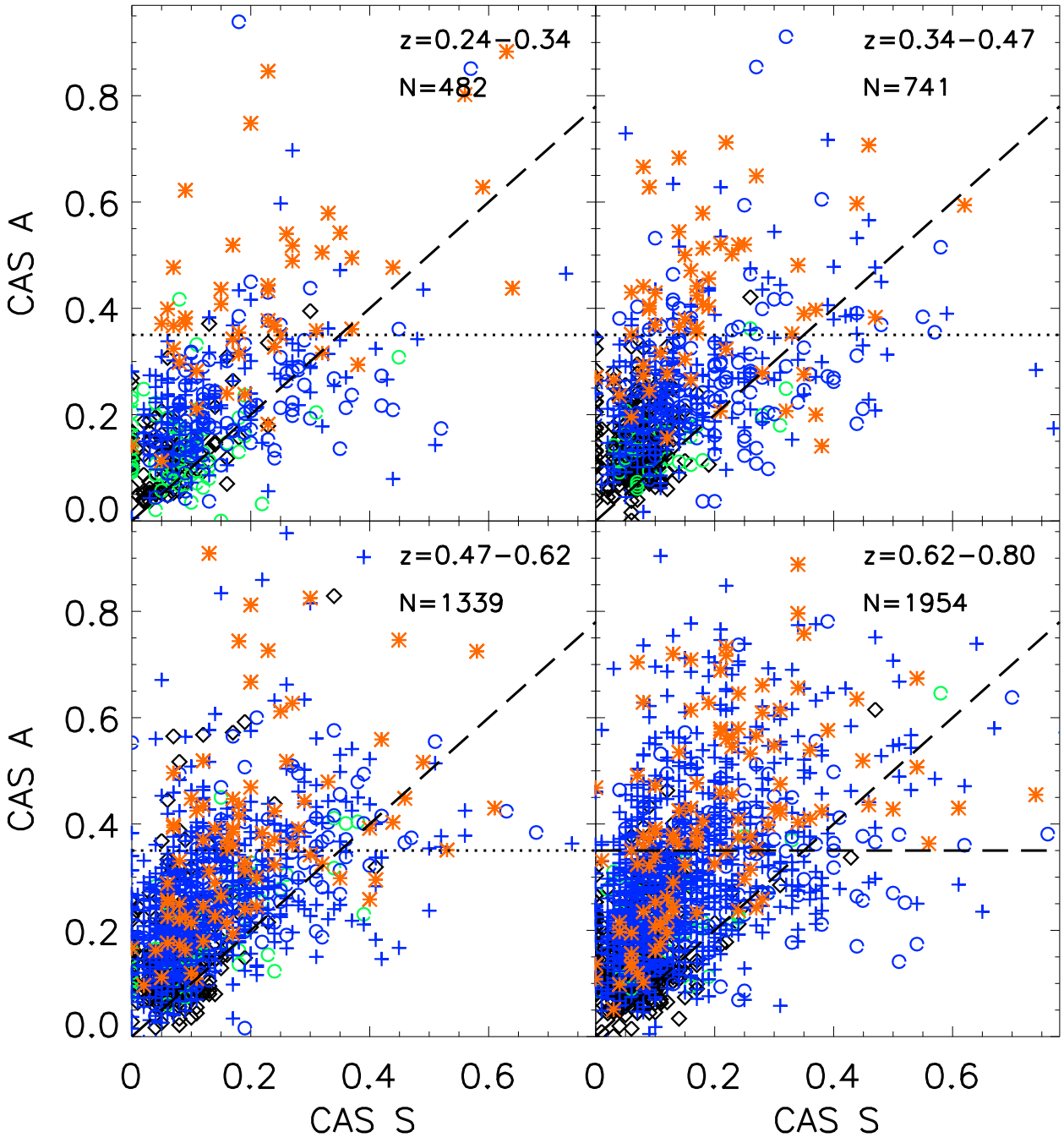

Fig. 8.— The CAS asymmetry A and clumpiness S parameters are plotted for galaxies in the four redshift bins of Fig. 1, using the same color coding. Galaxies satisfying the CAS criterion ($A > 0.35$ and $A > S$) lie in the upper left hand corner, bracketed by the $A = S$ diagonal line and the $A = 0.35$ horizontal line. The CAS criterion captures a fair fraction (40% to 50%) of the strongly interacting galaxies, but it also picks up "contaminants" in the form of normal non-interacting galaxies. This is further illustrated in Fig. 9.

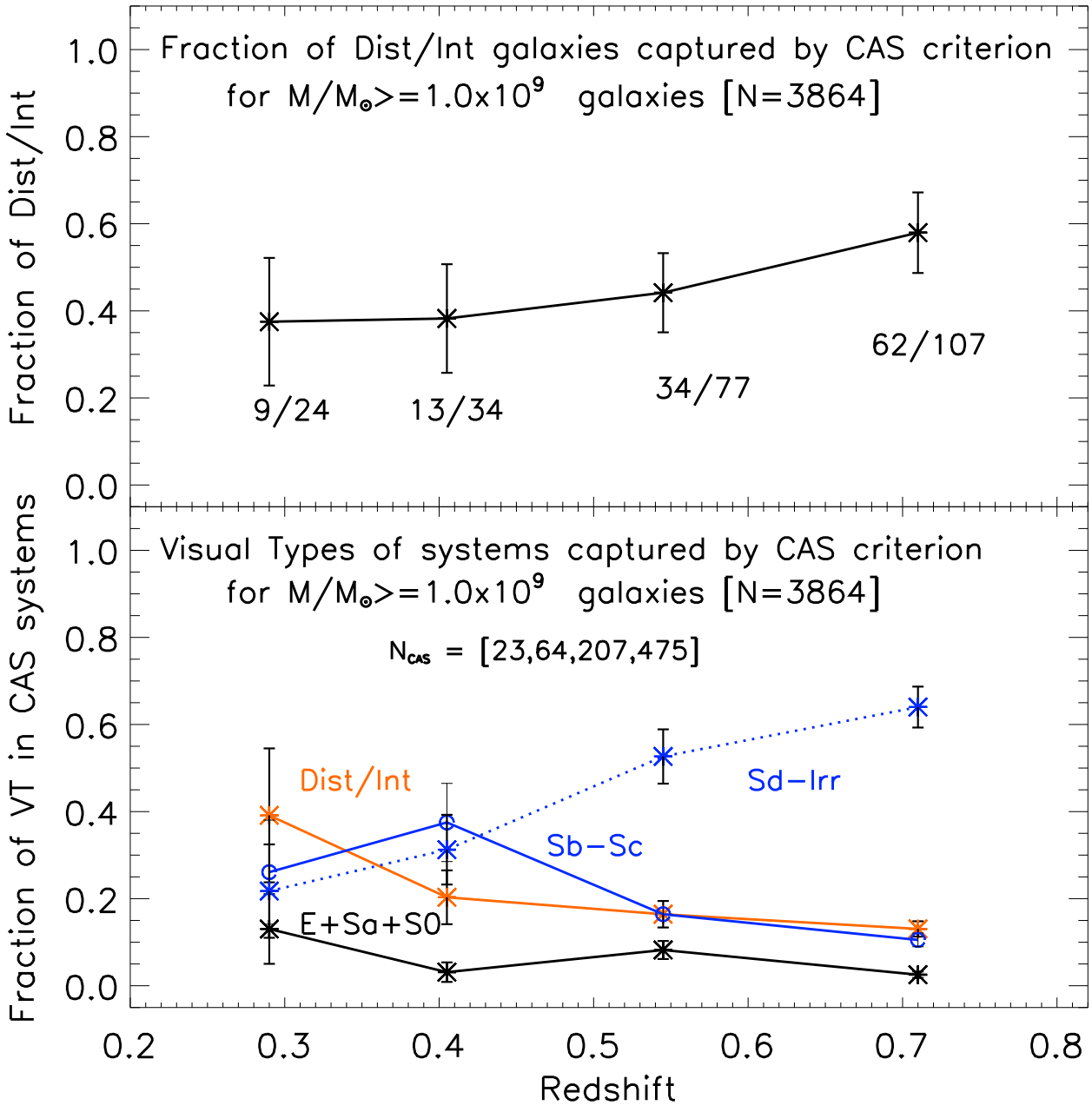

Fig. 9.— The top panel shows the fraction of strongly disturbed (Dist) systems captured by the CAS criterion ($A > 0.35$ and $A > S$) for the intermediate mass ($M/M_{\odot} \geq 1.0 \times 10^9$) sample. About 40% to 50% of the Dist systems are captured across the four redshift bins. The bottom panel shows the contamination level of the CAS system. $N_{\rm CAS}$ represents the number of systems picked up by the CAS criterion in the four redshift bins. The distribution of visual types among these systems is plotted. The vast majority (65% to 85%) of sytems picked up by CAS are normal non-interacting systems [Sd-Irr, Sb-Sc].

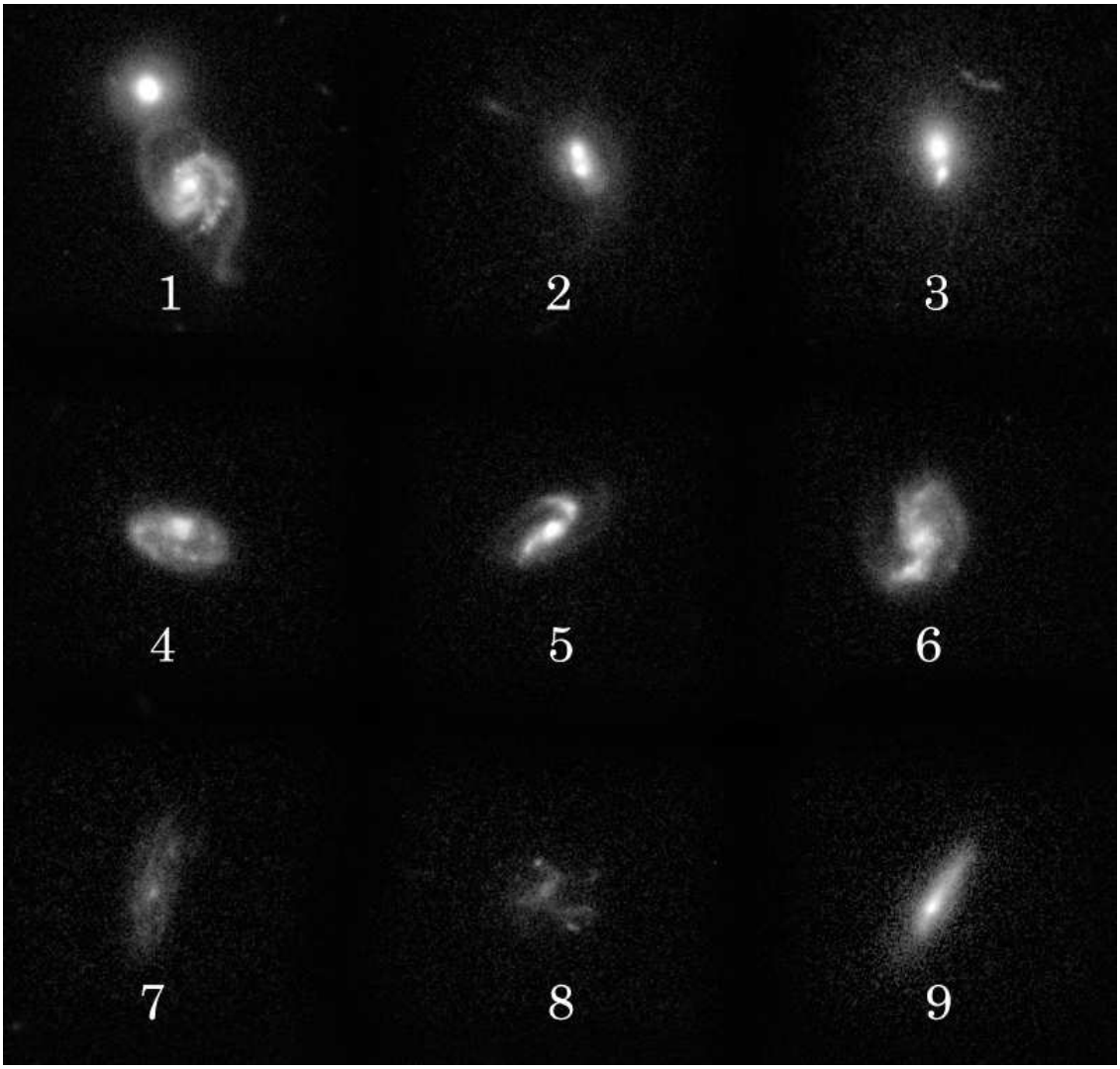

Fig. 10.— The montage shows typical systems where the CAS criterion ($A > 0.35$ and $A > S$) fails. Cases 1-3 are systems, which are visually classified as strongly interacting ('Int'), but are missed out by the CAS criterion. They include galaxies with tidal debris (Case 3), close double nuclei (case 2), and galaxies at the same redshift connected via tidal features (case 1). Conversely, cases 4-9 are systems, which are visually classified as non-interacting ('Normal') galaxies, but are picked by the CAS criterion. They include non-interacting, actively star-forming systems with small-scale asymmetries in the optical blue light (cases 4 and 6); systems where A is high due to the absence of a clear center (case 8) or due to the center being blocked by dust (case 4, 9); edge-on systems and compact systems, where the light profile is steep such that small centering inaccuracies lead to large A (case 9).

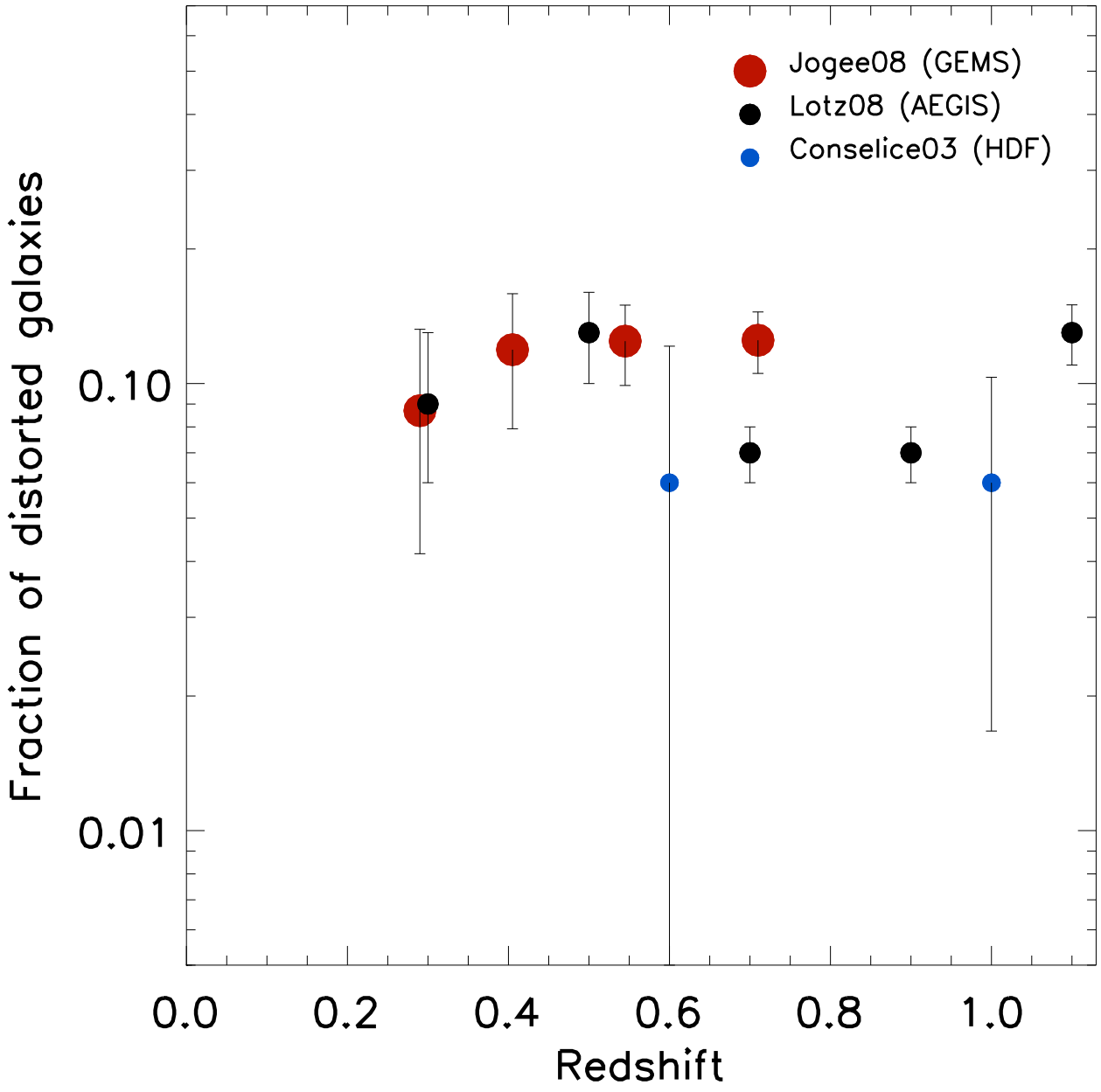

Fig. 11.— We compare our observed fraction f of strongly interacting galaxies in the high mass ($M \geq 2.5 \times 10^{10}$ $M_{\odot}$) sample to other studies, noting the caveats outlined in § 4.4. Shown here is the fraction of morphologically disturbed systems based on Gini-M20 parameters among $M_{\rm B}$ < -20.5 and $L_{\rm B} > 0.4$ L_{*} galaxies in the Extended Groth Strip (Lotz et al. (2008). The CAS-based results from Conselice (2003) are derived from a small sample in the Hubble Deep Field.

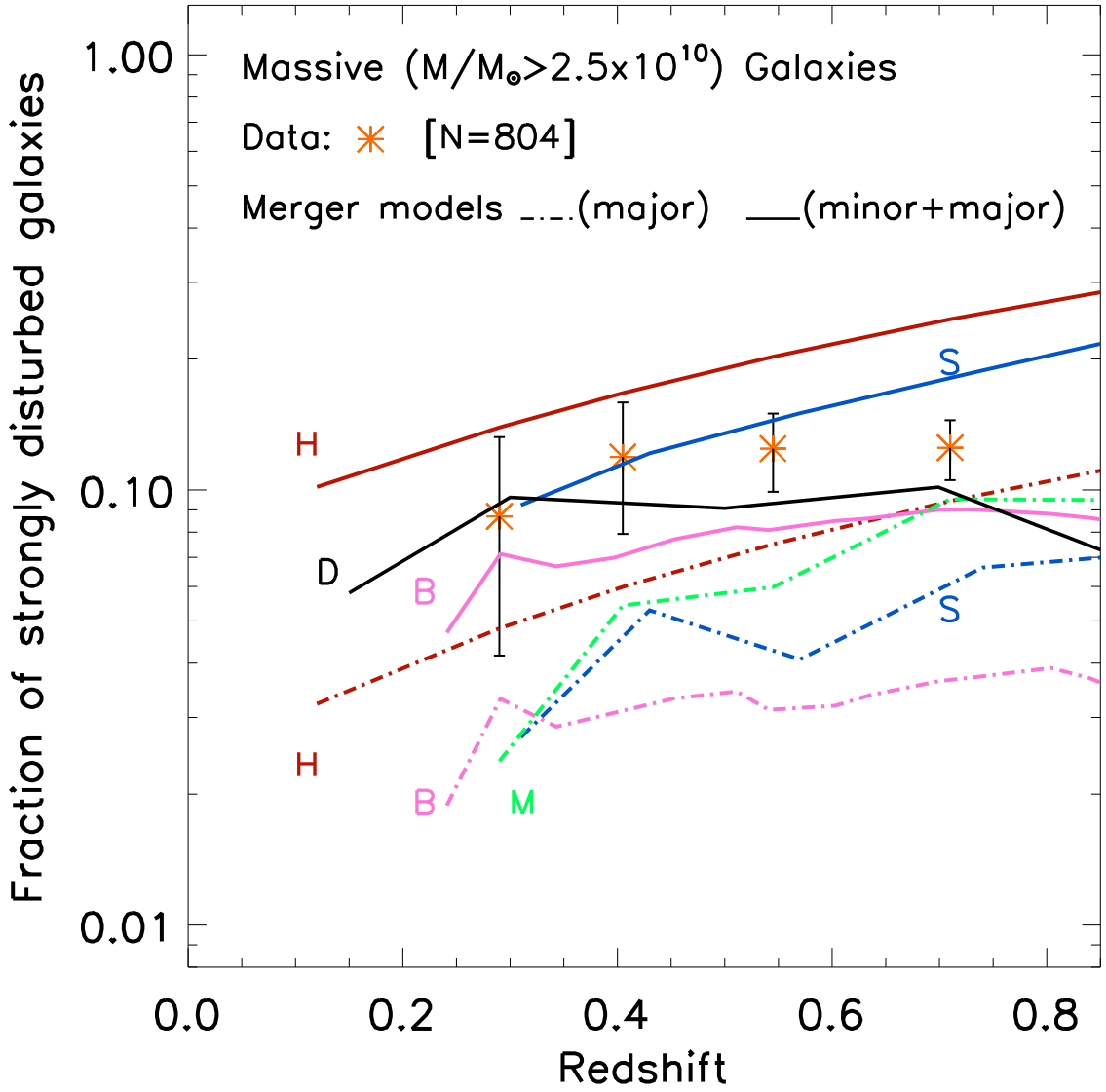

Fig. 12.— The observed fraction f of high mass strongly interacting galaxies (orange stars) is compared to merger fractions predicted by simulations of galaxy evolution in a ΛCDM cosmogony. The observed f represents an estimate of the fraction of recent/ongoing interactions of mass ratio $M1/M2 > 1/10$. It is compared to the model predictions for major+minor mergers (solid lines; $M1/M2 > 1/10$). Also shown are the model predictions for the fraction of major mergers ($M1/M2 \geq 1/4$; dotted-dashed lines). The models considered here include the semi-analytical models of Somerville et al. (in prep.; blue lines labeled 'S'), the semi-analytical models of Benson et al. (2005; pink lines labeled 'B'), the HOD models of Hopkins et al. (2007; red lines labeled 'H'), the cosmological N-body simulations of D'Onghia et al. (2008; dark line labeled 'D'), and SPH simulations of Maller et al. (2006; green line labeled 'M').

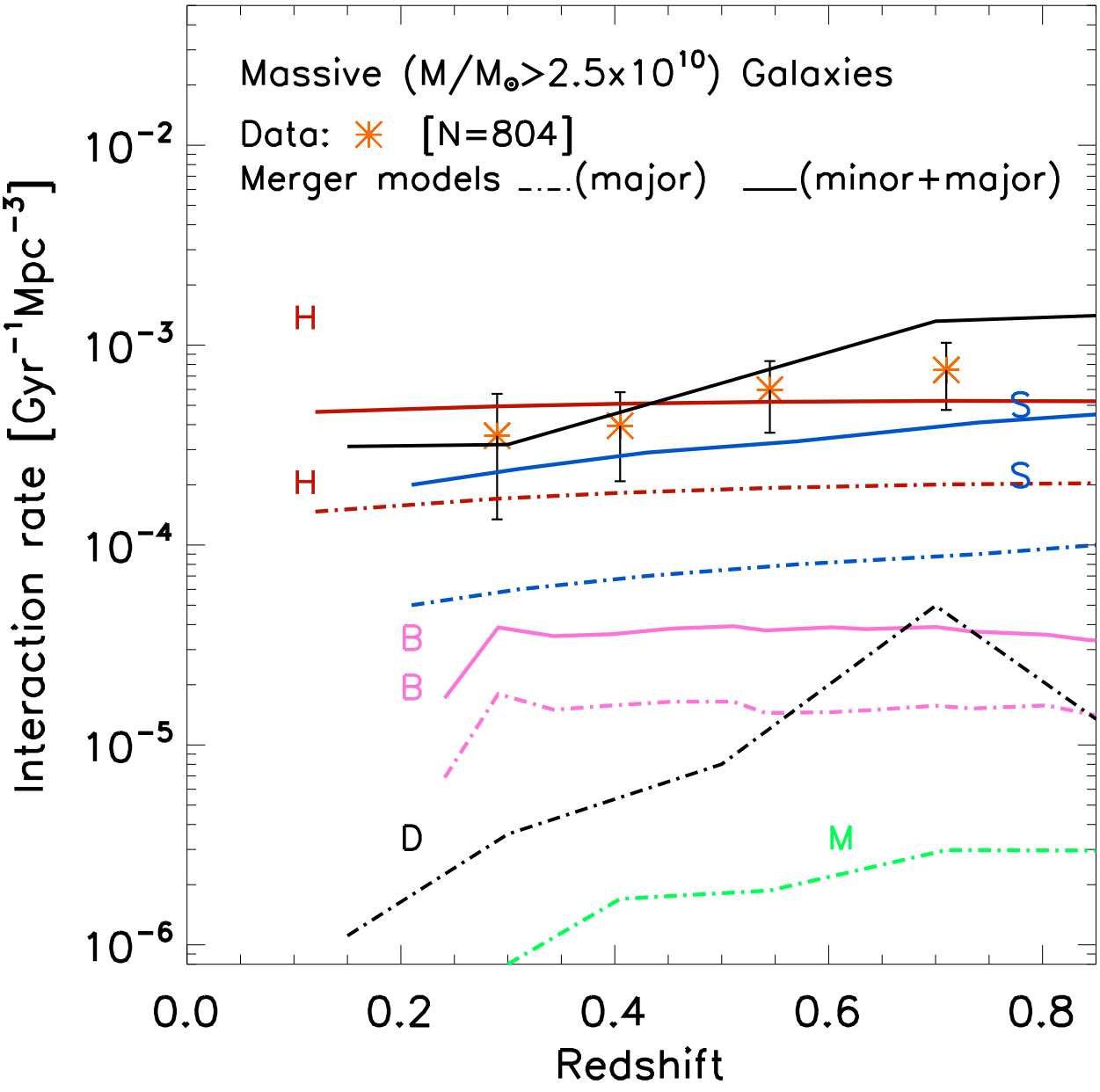

Fig. 13.— As in Fig. 12, but for the interaction rate R of high mass galaxies. Note that the model predictions can differ by over a factor of 30.

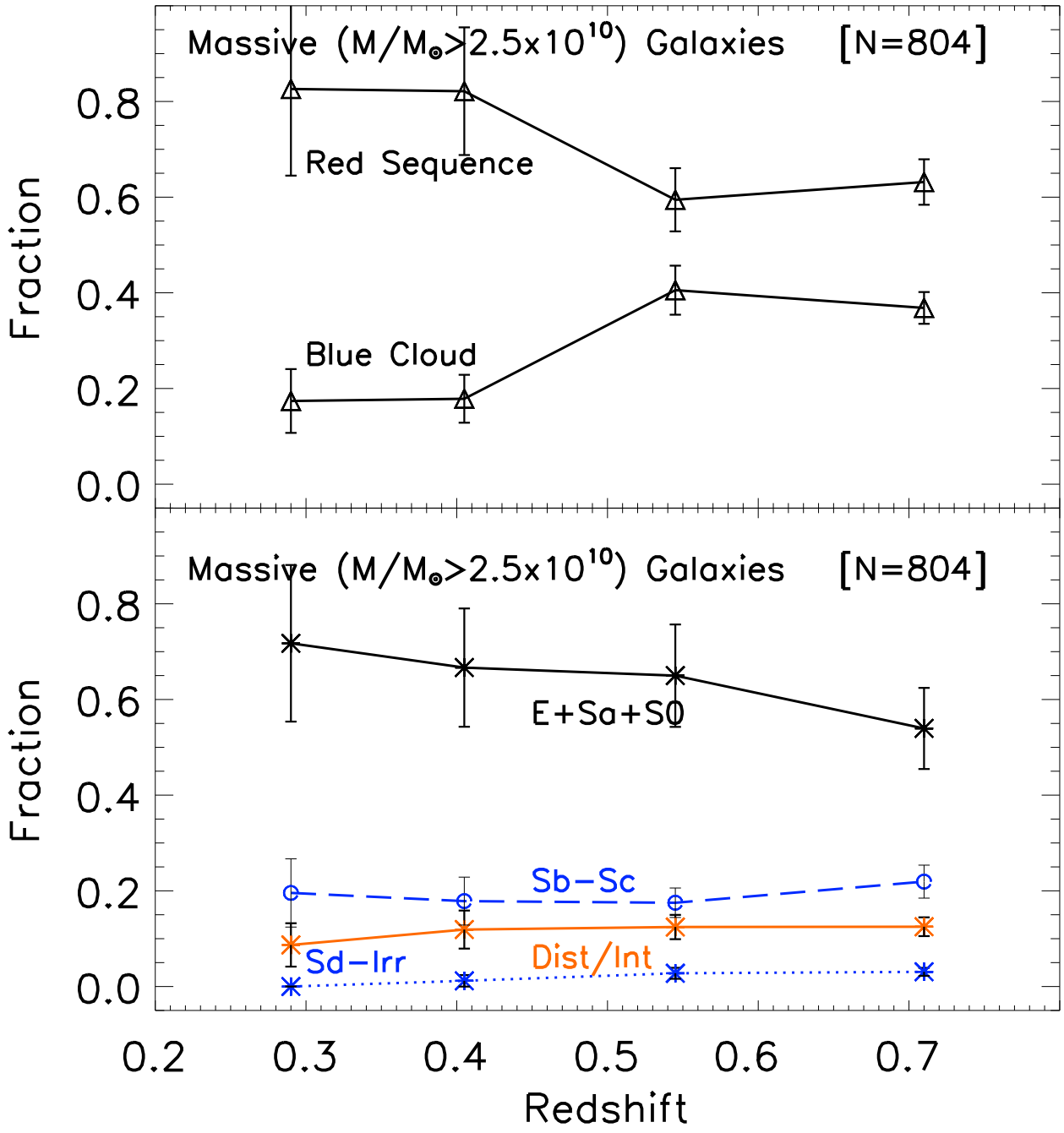

Fig. 14.— The top panel shows the fraction of galaxies in the blue cloud and red sequence as a function of redshift for the high mass ($M \geq 2.5 \times 10^{10}\ M_{\odot}$) sample (804 galaxies). The bottom panel shows the fraction of galaxies with different visual types: strongly interacting (Dist) and non-interacting (E+S0+Sa, Sb-Sc, Sd-Irr).

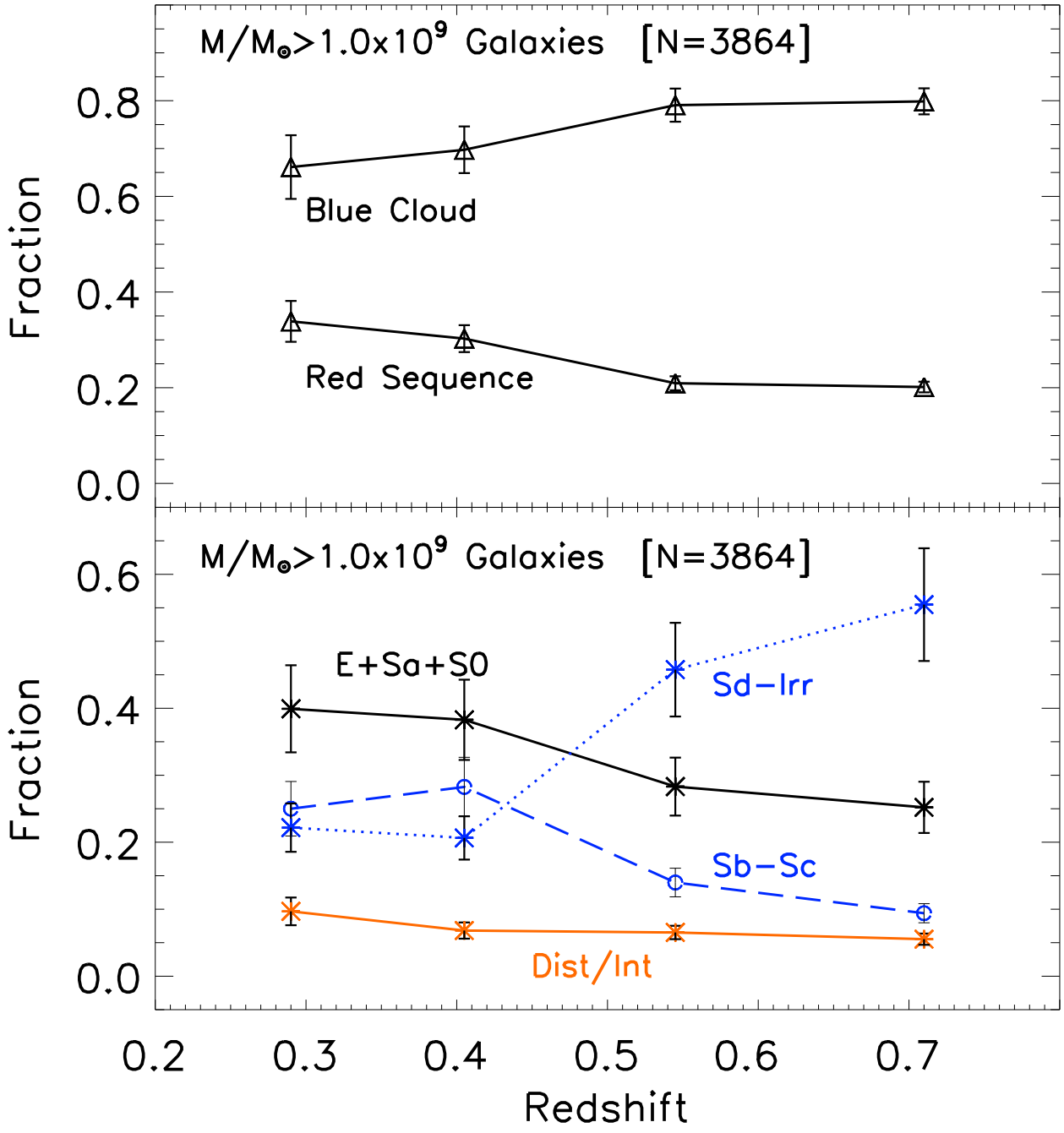

Fig. 15.— As in Figure 14, but for the intermediate mass ($M \geq 1 \times 10^9\ M_\odot$) sample. For this mass range, the red sequence is nearly complete only in the first redshift bin, while the blue cloud is complete over the entire interval $z \sim 0.24$–0.80.

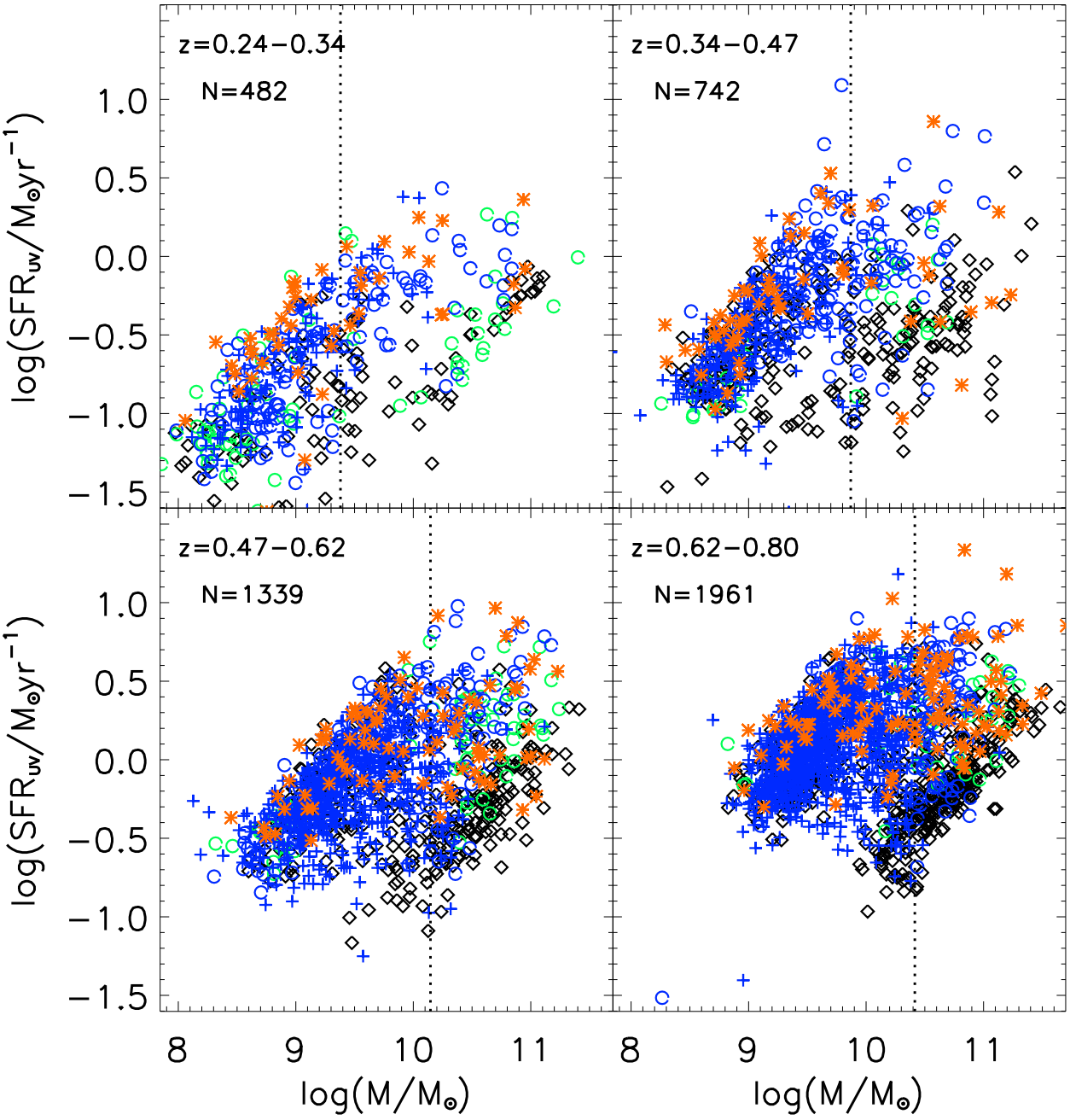

Fig. 16.— The UV-based star formation rate is plotted *versus* the stellar mass in four redshift bins, which span 1 Gyr each, and cumulatively cover the interval $z \sim 0.24$–0.80 ($T_{\rm back} \sim 3$–7 Gyr). N denotes the number of galaxies plotted in each bin. Galaxies are coded as in Fig. 1, with strongly interacting systems denoted by orange stars. The average SFR and total SFR density in both the UV and the IR, are further illustrated in Fig. 17 and Fig. 18.

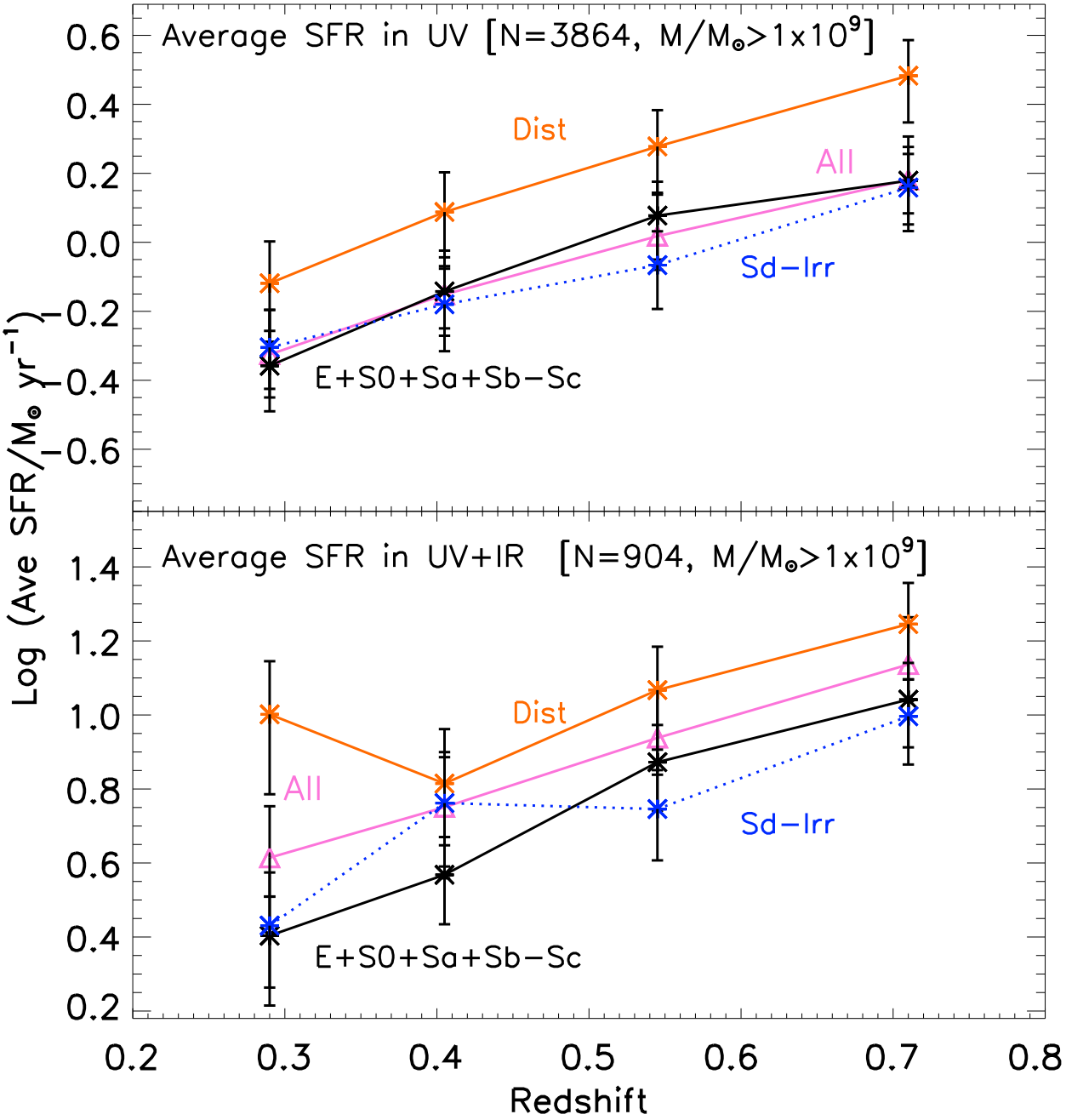

Fig. 17.— The average SFR of strongly interacting systems is compared to that of non-interacting E-to-Sc and non-interacting Sd-Irr, for four 1 Gyr redshift bins. N denotes the number of galaxies used. The average UV-based SFR (top panel) and average UV+IR-based SFR are only modestly enhanced in strongly interacting galaxies, compared to non-interacting galaxies over $z \sim 0.24$–0.80 (lookback time $\sim$ 3–7 Gyr).

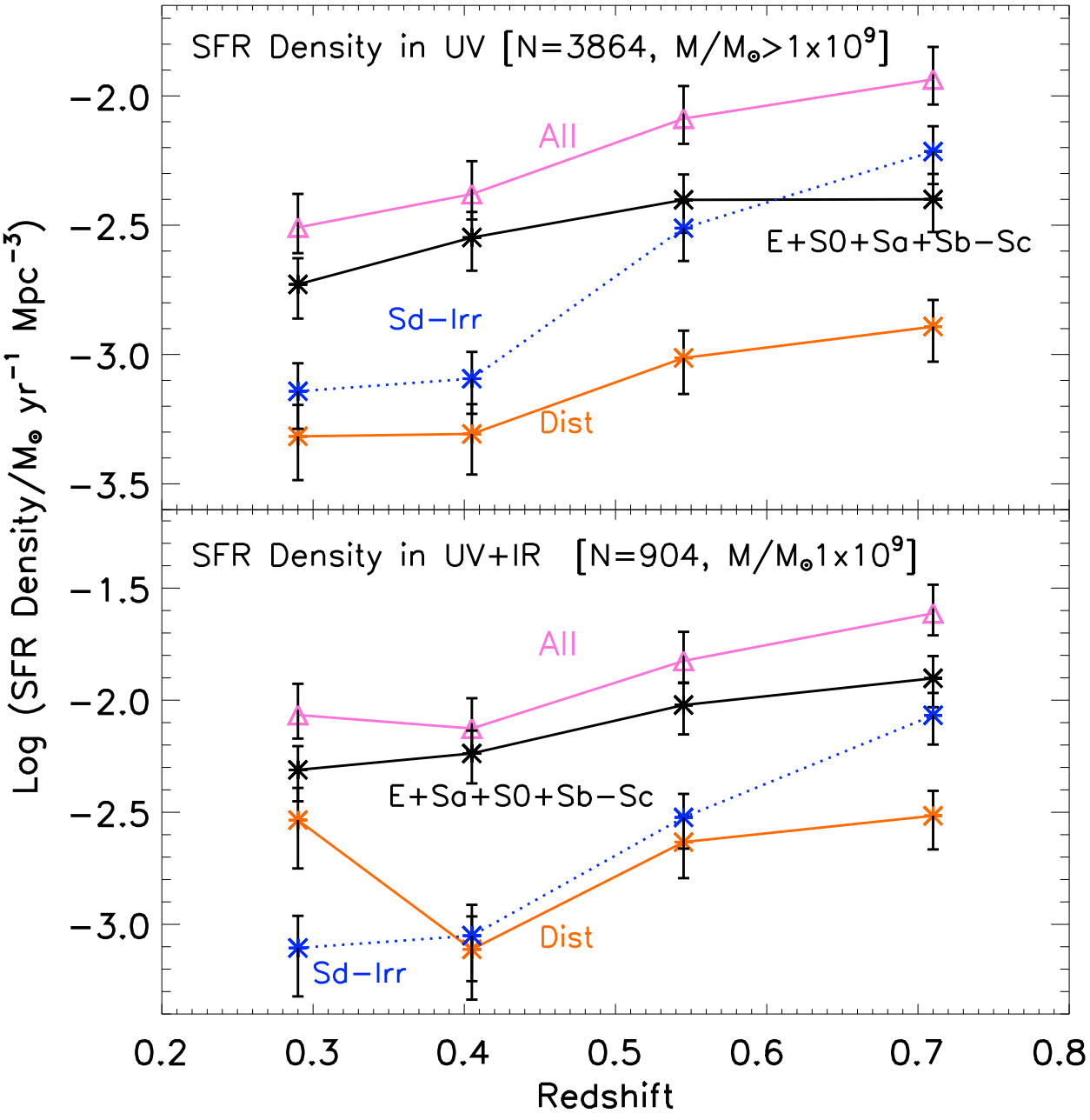

Fig. 18.— The plot of cosmic SFR density as a function of redshift (*aka* the Madau plot) over the last 3-7 Gyr is broken down into strongly interacting (Dist) galaxies and normal non-interacting galaxies (E+S0+Sa, Sb-Sc, Sd-Irr). N denotes the number of galaxies used. In all bins, strongly interacting galaxies only contribute a small fraction (typically below 20%) of the UV-based (top panel) or UV+IR-based (lower panel) cosmic SFR density, compared to normal non-interacting galaxies. In effect, the behavior of the cosmic SFR density over the last 7 Gyr is predominantly shaped by normal galaxies rather than strongly interacting galaxies.

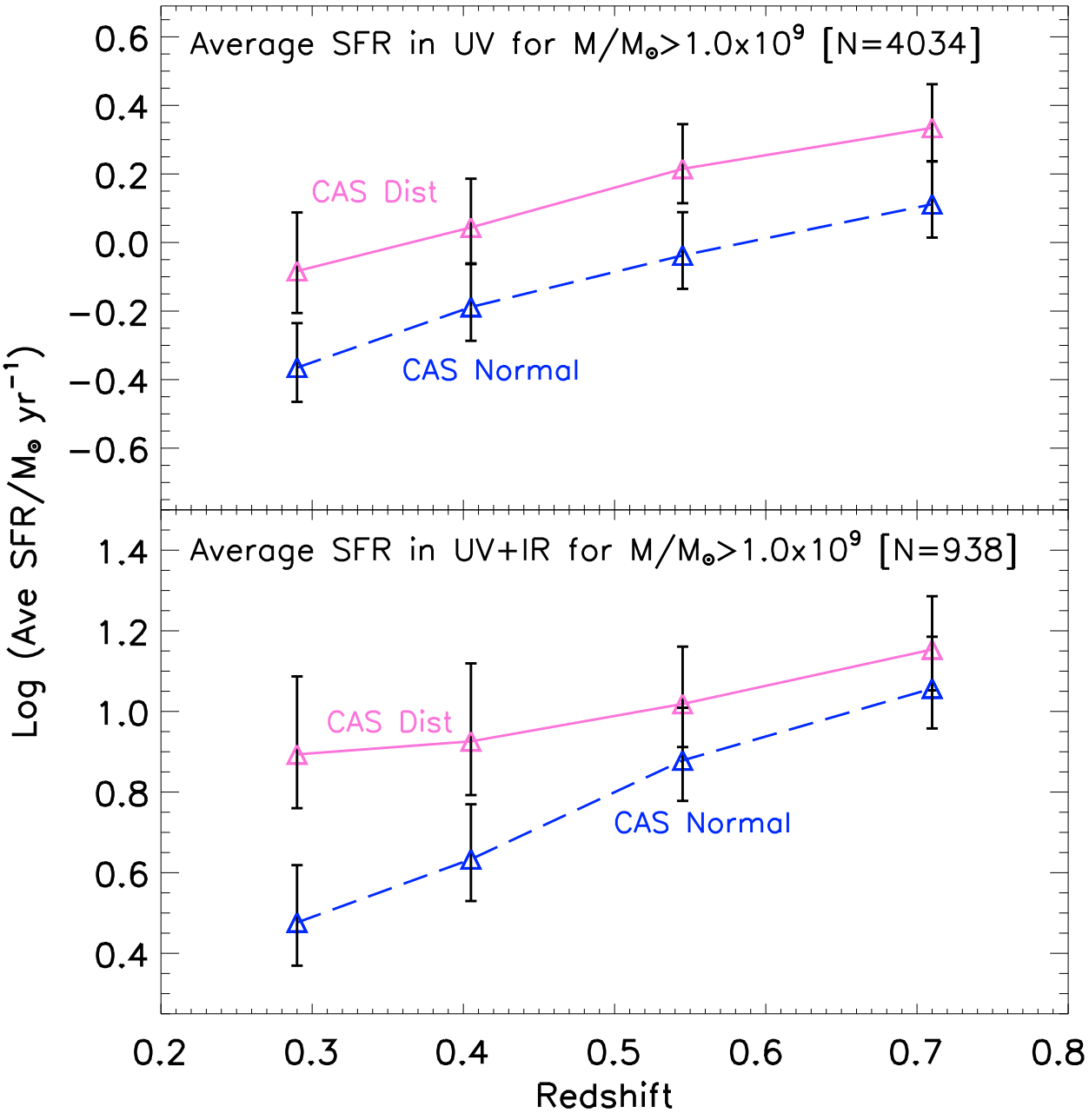

Fig. 19.— Same as in Fig. 17, but using the CAS criterion to identify strongly interacting galaxies.

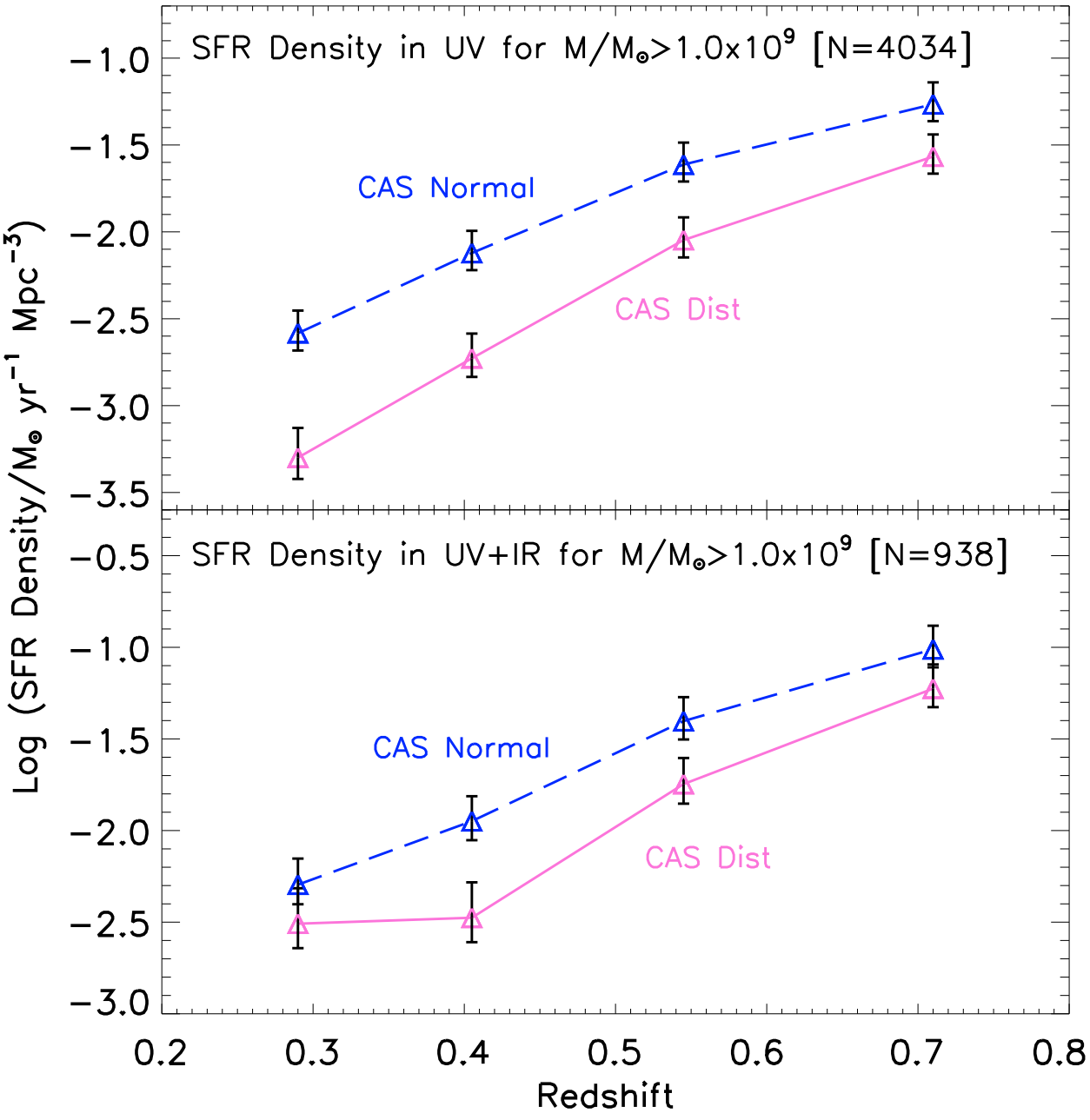

Fig. 20.— Same as in Fig. 18, but using the CAS criterion to identify strongly interacting galaxies.

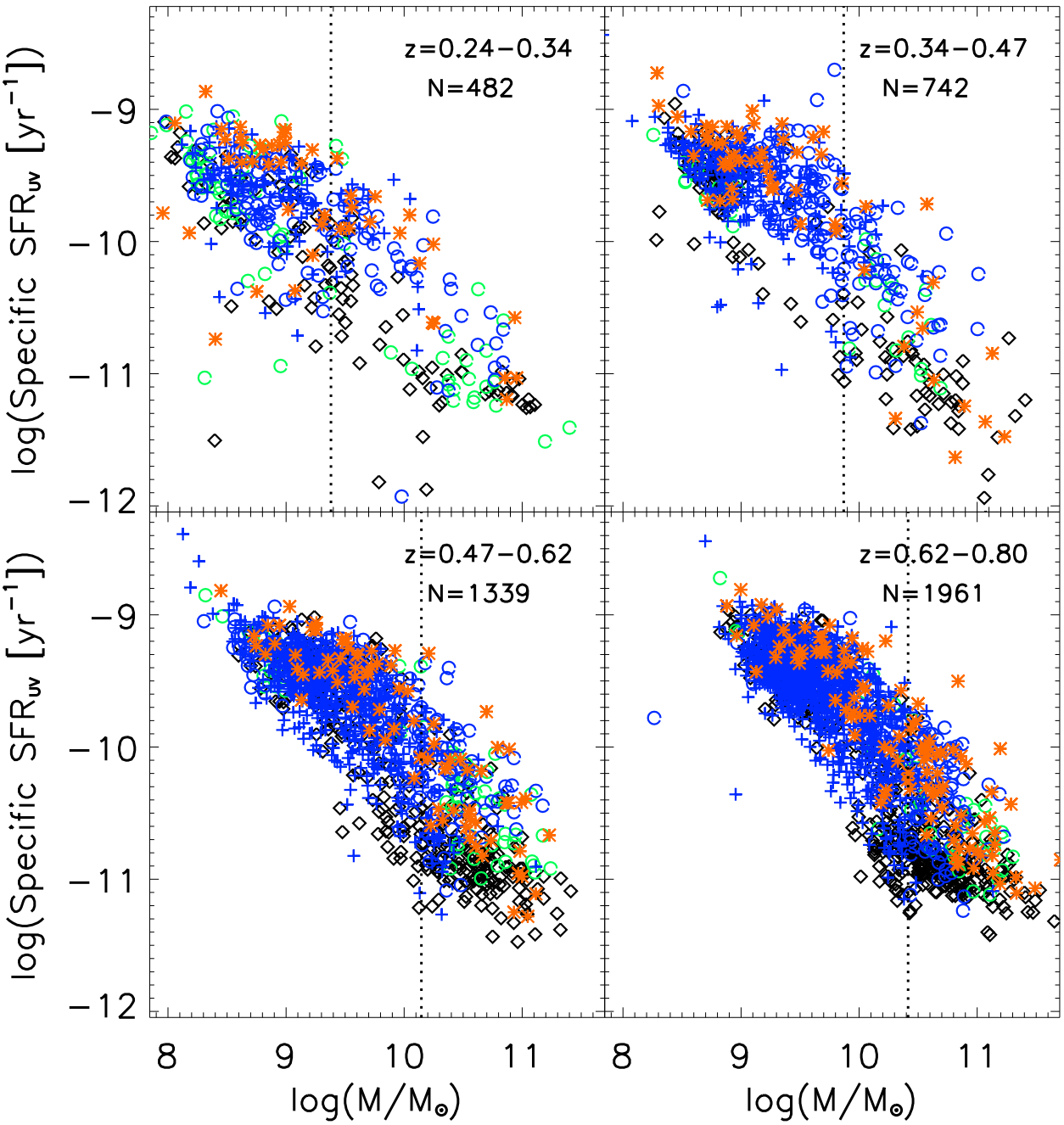

Fig. 21.— The specific SFR (defined as the SFR per unit stellar mass) based on UV data is plotted versus stellar mass. It ranges from 3×10^{-12} to 10^{-9} yr^{-1} and varies inversely with mass in all 4 redshift bins over $z \sim 0.24$–0.80. This is consistent with the idea that lower mass systems experience a larger fractional growth than high mass systems since $z < 1$, and that high mass systems have experienced the bulk of their stellar mass growth at earlier epochs ($z > 1$)

Table 1. Visual Types in F606W for Sample S1 [$M \geq 2.5 \times 10^{10}\ M_{\odot}$; N=804]

(1)	Redshift bin	1	2	3	4
(2)	Redshift range	0.24–0.34	0.34–0.47	0.47-0.62	0.62–0.80
(3)	Lookback time [Gyr]	3.0–4.0	4.0–5.0	5.0–.6-0	6.0–7.0
(4)	$\lambda_{\rm rest}$ in F606W [Å]	4470–4414	4414–4023	4023–3651	3651–3286
(5)	Total no of galaxies	46	84	217	456
(6)	Fraction of E+S0+Sa	0.717	0.667	0.650	0.539
(7)	Fraction of Sb-Sc	0.196	0.179	0.175	0.219
(8)	Fraction of Sd-Irr	0.000	0.012	0.028	0.031
(9)	Fraction of Dist	0.087	0.119	0.124	0.125
(10)	Fraction of Compact	0.000	0.024	0.023	0.086

Note. — Rows are : (1) Redshift bin. (2) Range in redshift covered by the bin; (3) Range in lookback time covered by the bin; (4) Range in rest-frame wavelength traced by the F606W filter over the bin, assuming a pivot wavelength of 5915Å; (5) to (10) Total number of galaxies and the fraction of these visually classified as E+S0+Sa, Sb-Sc, Sd-Irr, Dist, and Compact (see text);

Table 2. Visual Types in F606W for Sample S2 [$M \geq 1.0 \times 10^9\ M_\odot$); N=3860]

(1)	Redshift bin	1	2	3	4
(2)	Redshift range	0.24–0.34	0.34–0.47	0.47-0.62	0.62–0.80
(3)	Lookback time [Gyr]	3.0–4.0	4.0–5.0	5.0–.6-0	6.0–7.0
(4)	$\lambda_{\rm rest}$ in F606W [Å]	4470–4414	4414–4023	4023–3651	3651–3286
		All [N=3860]			
(5)	Total no of galaxies	248	499	1180	1937
(6)	Fraction of E+S0+Sa	0.399	0.382	0.283	0.252
(7)	Fraction of Sb-Sc	0.250	0.283	0.140	0.094
(8)	Fraction of Sd-Irr	0.222	0.206	0.458	0.555
(9)	Fraction of Dist	0.097	0.068	0.065	0.055
(10)	Fraction of Compact	0.032	0.060	0.054	0.044
		Blue Cloud [N=xxxx; TO BE UPDATED]			
(11)	Total no of galaxies	248	499	1180	1937
(12)	Fraction of E+S0+Sa	0.3992	0.3828	0.2831	0.2521
(13)	Fraction of Sb-Sc	0.2500	0.2826	0.1398	0.0940
(14)	Fraction of Sd-Irr	0.2218	0.2064	0.4576	0.5548
(15)	Fraction of Dist	0.0968	0.0681	0.0653	0.0553
(16)	Fraction of Compact	0.0323	0.0601	0.0542	0.0439

Note. — Rows are : (1) Redshift bin. (2) Range in redshift covered by the bin; (3) Range in lookback time covered by the bin; (4) Range in rest-frame wavelength traced by the F606W filter over the bin, assuming a pivot wavelength of 5915Å; (5) to (10) Total number of galaxies and the fraction of these visually classified as E+S0+Sa, Sb-Sc, Sd-Irr, Dist, and Compact (see text);

Table 3. Test for bandpass shift and surface brightness dimming

	Strongly-interacting ('Int')	Non-interacting ('E-Sd')	Non-interacting ('Irr')
GEMS F606W			
Deep GOODS F850LP			
GEMS/GOODS			

Note. —